SAPIENZA
Università di Roma
Facoltà di Farmacia e Medicina

Ph.D. in
MORPHOGENESIS AND TISSUE ENGINEERING

XXXVI Ciclo
(A.A. 2022/2023)

"Enhancing sensitivity of triple-negative breast cancer to DNA damaging therapy through chemical inhibition of the m^6A methyltransferase METTL3"

Ph.D. Student
Bianca Cesaro

Tutor
Prof. Francesco Fazi
Prof. Alessandro Fatica

Coordinator
Prof. Antonio Musarò

CONFIDENTIALITY NOTICE

Reviewers and PhD committee members are obliged to keep the files confidential and to delete all records after completing the review process.

The submission of scientific works for the attainment of the Doctor of Philosophy degree, as a Member of the Faculty Board of the Doctorate in Morphogenesis and Tissue Engineering, requires adherence to the following regulations:

i. Treat confidential and sensitive information as strictly private and undertake all reasonable measures to maintain such confidentiality.

ii. Utilize confidential and sensitive information solely for the purposes for which it has been provided or disclosed, committing not to disclose to third parties any information contained in the received works.

iii. Ensure the utmost confidentiality, in compliance with current regulations on trademarks, copyrights, and patents for industrial inventions, as well as privacy regulations pursuant to Legislative Decree 196/2003. This applies to know-how and all acquired information, which may under no circumstances, for any reason, be used for personal or others' gain, disclosed, reproduced, or otherwise made known to third parties.

INDEX

1. SUMMARY

The biological issue. Among the different types of breast cancer, triple-negative breast cancer (TNBC) displays the most unfavourable prognosis and high risk of recurrence. Conventional chemotherapy and DNA damaging agents are the main treatment for this cancer. However, this tumor subtype is characterized by high heterogeneity and therapy resistance issues, which constantly demands for novel strategies of treatment.
Since TNBC presents high m^6A methyltransferase METTL3 activity, which correlates with invasiveness and metastasis, we proposed to evaluate the impact of m^6A depletion through METTL3 chemical inhibition using STM2457 small-molecule.
Results. Here, we show that STM2457, a selective METTL3 catalytic inhibitor, strongly affects TNBC cell proliferation and migration *in vitro* and *in vivo*. Moreover, STM2457 sensitizes tumor cells to DNA damaging agents utilized in TNBC therapy, such as platinum-salts and the PARP1/2 inhibitor olaparib. Finally, we show that the catalytic inhibition of METTL3 synergizes with DNA-damaging chemotherapy in TNBC patient-derived organoids with wild-type BRCA1 and BRCA2 genes.
Conclusions. Taken together, our data suggests that incorporating small-molecule inhibitors of METTL3 into standard treatment for TNBC holds significant promise, opening avenues for innovative combination targeted therapies. This approach has the potential to enhance anti-cancer efficacy and mitigate the risk of toxicities.

2. INTRODUCTION

2.1 N^6-methyladenosine (m^6A)

N^6-methyladenosine (m^6A) consists in the addition of a methyl group (CH_3) to the nitrogen atom at the sixth position of the adenine base within an RNA molecule, therefore it belongs to the field of epitranscriptomics. Among more than 160 post-transcriptional chemical modifications identified on RNA, N^6-methyladenosine is the most abundant internal modification in polyadenylated-mRNAs and long non-coding RNAs in higher eukaryotes. However, rRNAs, snRNAs and tRNAs also contain m^6A.

In the early 1970s, studies on post-transcriptional RNA modifications were a topic of growing interest in biological research. In parallel to the discoveries of 7-methylguanosine (m^7G) cap structure identified at the 5' end of messenger RNA transcripts and ribosomal RNA, N^6-methyladenosine was first discovered in mRNAs. Friderici and Rottman's group were conducting studies in rat hepatoma cells, in a time where mRNAs from eukaryotes were only known to contain a 3'-terminal poly(A) sequence. In these studies, RNA was methyl-labeled with 3H-methionine, mRNA was purified with oligo dT-cellulose, digested and nucleotides were separated by high-speed liquid chromatography. While ribosomal RNA and tRNA possessed complex base-methylnucleoside patterns, the distribution in mRNA was quite simple, consisting predominantly of N^6-methyladenosine, demonstrating a unique distribution of methylated nucleosides in mRNA[1].

Within a few months after the initial discovery, other research groups conducted studies on this modification[2], including Adams and Cory's group which carried out preliminary experiments to map the position of m^6A in mouse myeloma cells[3], which was found to be located within the coding portion of m RNA. They also advanced the hypothesis that since m^6A hydrogen bonding

properties might interfere with translation, positions within the non-coding regions were preferably favored, as 5'-terminal region and a region preceding the poly(A) sequence (3'-UTR).
In 2012, a consistent development in the field of epitranscriptomic leading to m^{6}A-seq by Dominissini et al.[4] and MeRIP-seq by Meyer et al.[5] found that modified adenosines are specifically enriched in regions adjacent to the stop codon, 3′-UTR and within long internal exons. Furthermore, the first evidence that the internal m^{6}A residues are present in a specific sequence in that residues are preceded by adenosine or guanosine and followed exclusively by cytosine[6], led to the identification of the m^{6}A consensus sequence as DRACH motif (D = A/G/U, R = A/G; H = A/C/U) where the A is the methylated nucleotide. There are ∼3 m^{6}A residues per average mRNA transcript in mammalian cells[4], meaning that only about 20% of consensus motifs are methylated, thus suggesting that the modification is deposited in specific regions of mRNAs.
The discoveries obtained so far are results of experiments performed in mammals, but m^{6}A was subsequently identified in Zebrafish[7], Drosophila melanogaster[8], plants[9,10,11,], yeast[12] and viruses[13,14]. These findings indicate that m^{6}A modification is conserved throughout evolution and underlies its crucial biological functions.

2.2 m^{6}A players: "writers", "erasers" and "readers"

m^{6}A is co-transcriptionally deposited[15] on RNA by the RNA methyltransferase METTL3 (methyltransferase-like protein 3)[16]. METTL3 forms a heterodimer with METTL14 (methyltransferase-like protein 4)[17], establishing the m^{6}A-METTL complex (MAC). METTL14 has no catalytic activity but it functions as an RNA-binding scaffold and facilitates METTL3 allosteric (Figure 2.1).

Furthermore, the MAC complex is supported by associated proteins (WTAP, VIRMA, RBM15/15B, ZC3H13 and HAKAI)[18] forming a large protein complex named MACOM (m^6A-METTL-associated complex) which contributes to stabilizing the whole complex. Moreover, these adaptor proteins may help in determining the specific sites of m^6A methylation. Indeed, VIRMA mediates preferential m^6A mRNA methylation in the 3'UTR, while HAKAI affects m^6A modification distributed in the 5'UTR[19]. In details, the methyltransferase METTL3 contains the subunit which catalyzes the transfer of a methyl group (CH3) from a methyl donor molecule, S-adenosylmethionine (SAM) to the adenosine (GCACU) in the RNA molecule. Although most of the mRNAs are methylated by the METTL3-METTL14 complex, m^6A is also found in other RNA species, which is deposited by other RNA methyltransferases, or else named "m^6A writers". Among those, m^6A on 28S and 18S rRNA is the result of ZCCHC4 and METTL5-TRMT112 complex activity, respectively. METTL16 mediates m^6A modification in U^6 snRNA and a small proportion of other mRNAs through specific structural recognition[19].
Since the biological function of RNA modifications, including m^6A, is to regulate processes that involve rapid expression changes of genes and proteins[21] it was conceivable to imagine these modifications to be reversible and dynamic. Indeed, in 2011, the first m^6A demethylase fat mass and obesity-associated protein (FTO) was discovered[22]. After 2 years, a second m^6A demethylase alkB homolog 5 (ALKBH5) was discovered[23]. These two demethylases, also called "m^6A erasers", share their FeII/α-KG-dependent dioxygenase nature but they are differentially expressed. FTO is enriched in the brain while ALKBH5 is predominantly expressed in testis. Furthermore, FTO is a promiscuous demethylase as it can also demethylate the N^6-2'-O-dimethyladenosine (m^6Am) modification, which is mostly present in close proximity to the 5' cap structure[24].
Within the dynamism that characterizes m^6A deposition and removal, this mark is recognized by several RNA-binding proteins

that read this modification and therefore are named "m^{6}A readers". These proteins regulate the fate of RNA, by controlling different aspect of RNA metabolism, including splicing, nuclear export, cytoplasmic stability and translation[25–27].

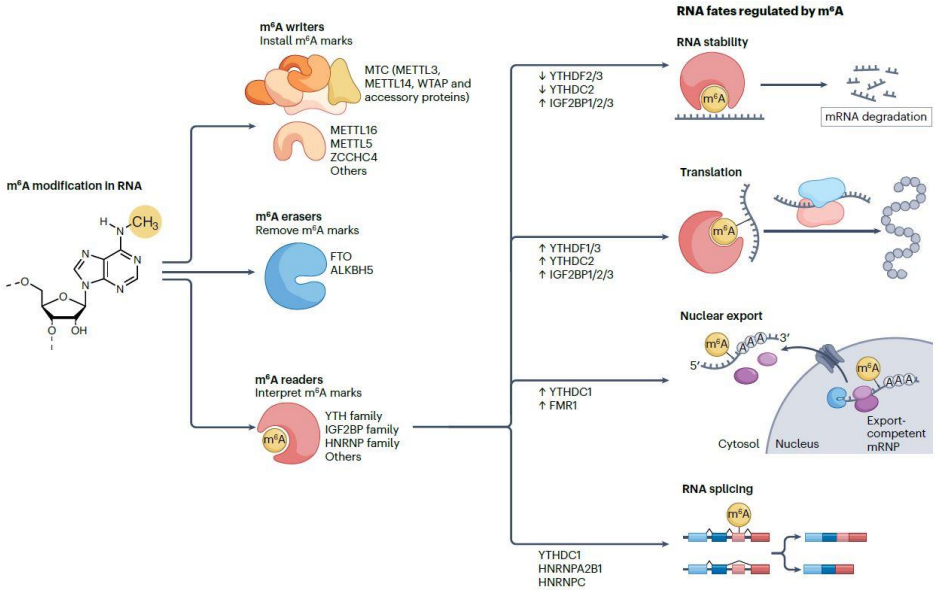

Figure 2.1. N^6-Methyladenosine (m^{6}A) methylation of messenger RNAs (mRNAs) is primarily orchestrated by the m^{6}A methyltransferase complex (MTC), which comprises a core complex (METTL3 and METTL14) and additional accessory subunits. FTO and ALKBH5 demethylases are responsible for the removal of methyl groups from m^{6}A-modified RNAs. Various m^{6}A reader proteins, YTHDF/YTHDC, IGF2BP, and HNRNPs recognize m6A marks. These reader proteins mediate diverse processes that influence the fate of their target RNAs, encompassing RNA splicing, nuclear export, translation, and stability[20].

The YT521-B homology (YTH) domain family of proteins (YTHDF1, YTHDF2, YTHDF3 and YTHDC1) have been characterized as direct m^{6}A readers and have a conserved m^{6}A-binding pocket[4]. While YTHDC1 acts in proximity of nuclear

speckles, which are transcription active site, by regulating RNA splicing and favoring nuclear export [25,28], YTH family of proteins are found in the cytoplasm and their recognition of the m^{6}A-transcript has been associated to different fate. Indeed, YTHDF1 is known to promote mRNA translation by recruiting the translation initiation factor complex 3 (eIF3)[27], YTHDF2 is capable of destabilizing m^{6}A-containing RNA through direct recruitment of the CCR4–NOT deadenylase complex[29], whereas YTHDF3 facilitates translation and decay of N^6-methyladenosine-modified RNA by forming heterodimers with YTHDF1 and YTHDF2, respectively[30].

However, in 2020, the prevailing model was doubted in favor of a new vision of the three YTHDF paralogs, which were shown to bind the same m^{6}A-modified mRNAs rather than different mRNAs[31]. To date, since YTHDFs exhibit high sequence homology, indeed, m^{6}A function might be a result of the combined action of YTHDF proteins in proportion to the number of m^{6}A sites. Furthermore, there are present in nature other m^{6}A readers which do not belong to the YTH family. For example, YTHDC2 is instead a member of DExD/H box RNA helicase family which was found to regulate mammalian spermatogenesis[32]. Insulin-like growth factor-2 mRNA-binding proteins 1, 2, and 3 (IGF2BP1–3) are reported as a novel class of m^{6}A readers and use K homology (KH) domains to selectively recognize m^{6}A-containing RNAs and promote their stability and translation[33]. Additionally, heterogeneous nuclear ribonucleoproteins (hnRNP C/G, A2B1) can bind m^{6}A-methylated RNAs which are altered by m^{6}A marks. Indeed, the structural switch called "m^{6}A switch" due to the presence of m^{6}A facilities the binding of indirect "m^{6}A readers", such as hnRNPs, promoting pre-mRNA processing[34].

Finally, although m^{6}A modification does not prevent Watson-Crick base pairing of A-U nucleotides, m^{6}A residues can affect tertiary interactions involving Hoogsteen base pairs that use the N^6 atom of A in the hydrogen bond. Therein, structural change in transcripts

due to altered Hoogsteen base pairing might favor or inhibit the binding of specific proteins[35].

2.3 m^{6}A biological relevance in development

A large body of evidence shows that m^{6}A methyltransferase mutations have crucial outcomes in many species. In mice, knocking out either METTL3 or METTL14 in embryonic stem cells (ESCs) causes inadequate termination of their naive cell state and resistance to differentiation, leading to early embryonic lethality (E5.5-E7.5)[36]. In murine[37] and zebrafish[38] oocytes, METTL3 mutations led to arrest in early developmental stage, suppressed maturation and caused defects in the maternal-to-zygotic transition. METTL3 was found to have a role in sex determination in Drosophila, as METTL3 mutants prevented female dosage compensation[39]. Additionally, knocking down METTL3 (or RBM15) was proven to impair XIST-mediated transcriptional silencing of genes on the X chromosome[40]. Conditional deletion of METTL3 in BMSCs resulted in incompetent osteogenic differentiation potential, reduced bone mass and impaired bone formation[41]. Loss of FTO leads to postnatal growth retardation and a significant reduction in adipose tissue and lean body mass[42]. Moreover, m^{6}A plays also important role in mouse adult brain, by regulating synaptic function[43] and stress-induced responses[44] and, consistently, has a fundamental function in the hematopoietic system, by controlling stem cell differentiation and homeostasis[45–47].

2.4 Triple-Negative Breast Cancer (TNBC)

In 2023, breast cancer still represents the most commonly diagnosed cancer in women, epidemiological evidence estimates

2.3 million new cases and >685,000 deaths reported in 2020 worldwide[48]. The underlying causes and factors that contribute to the development of the tumor are both genetic and non-genetic, which include age, exogenous female hormones, lifestyle factors (obesity, smoking, alcohol consumption)[49]. Over the years, an approach to comprehensively study breast cancer was to create classifications that incorporate considerations of histology, morphology, and molecular features. This approach aims to provide a more holistic understanding of the disease by integrating visual characteristics, cellular structures, and genetic/molecular profiles.

Breast tumors classified by histology are divided as *in situ* carcinoma or invasive carcinomas, based on the extent of malignant cell invasion from breast lobules or ducts into the surrounding stroma[50]. The most common form of pre-invasive breast cancer is ductal carcinoma in situ (DCIS) (80%), while invasive carcinomas are further subdivided according to cell morphology in invasive ductal carcinoma (IDC) (60%–75%), followed by invasive lobular carcinoma (ILC) (10%–15%)[51]. First pioneering microarray profiling performed in the 2000s identified five primary intrinsic molecular subtypes: luminal A, luminal B, HER2-enriched (Human Epidermal growth factor Receptor 2), basal-like, and claudin-low[52,53]. Luminal A tumors are ER+ (Estrogen Receptor) and/or PR+ (Progesteron Receptor), they express genes associated with luminal epithelial cells and typically have low proliferative rates. These tumors are associated with better prognosis, as hormone-targeted therapies result more effective here compared to other subtypes. Luminal B tumors are also ER+ and/or PR+, but have higher proliferative rates and worse prognosis than luminal A tumors. They exhibit higher expression of proliferation-related genes. HER2-enriched (HER2-E) tumors are characterized by HER2/ERBB2 amplification on chromosome 17q12 and intermediate expression of the luminal gene signature. These tumors might respond to targeted therapies that block HER2 signaling, such as trastuzumab (Herceptin). Basal-like tumors are

highly proliferative and display augmented expression of basal cytokeratins and EGFR and low expression of the luminal. Basal-like tumors are typically triple-negative, meaning they lack ER, PR, and HER2 expression. For this reason, hormone-targeted therapies are not effective on these tumors. The least frequent subtype, claudin-low tumors show enrichment in mesenchymal features and immune cell infiltrate, are also triple-negative and are characterized by low expression of tight junction proteins (claudins)[52,53].

Finally, histological and immunohistochemical features identify the major clinical subtypes of breast cancer: ER+ (70%), HER2+ (15%), and TNBC (15%) according to expression of the estrogen receptor (ER), progesterone receptor (PR), and human epidermal growth factor receptor 2 (HER2/ERBB2)[51](Figure 2.2).

Tumors lacking the expression of ER, PR, and HER2 are named TNBC and, therefore, they do not benefit from hormonal therapies targeting these receptors. TNBC accounts for about 15-20% of all breast cancers and is commonly diagnosed in younger women and in certain racial and ethnic groups, such as African American and Hispanic populations. It is often considered the most invasive and aggressive, with high recurrence and metastasis to lung and brain, compared to other breast cancer subtypes with a life expectancy of five years after diagnosis[54].

In 2011, Lehmann's classification was one of the first attempt to classify TNBC, which identified six distinct molecular subtypes of TNBC based on gene expression profiles: basal-like A (BL1), basal-like B (BL2), immunomodulatory (IM), mesenchymal (M), mesenchymal stem-like (MSL), and luminal androgen receptor (LAR)[55]. In details, basal-like A (BL1) has epithelial features and was keratin 5 and 14 positive, while basal-like B (BL2) has mesenchymal features including vimentin expression.

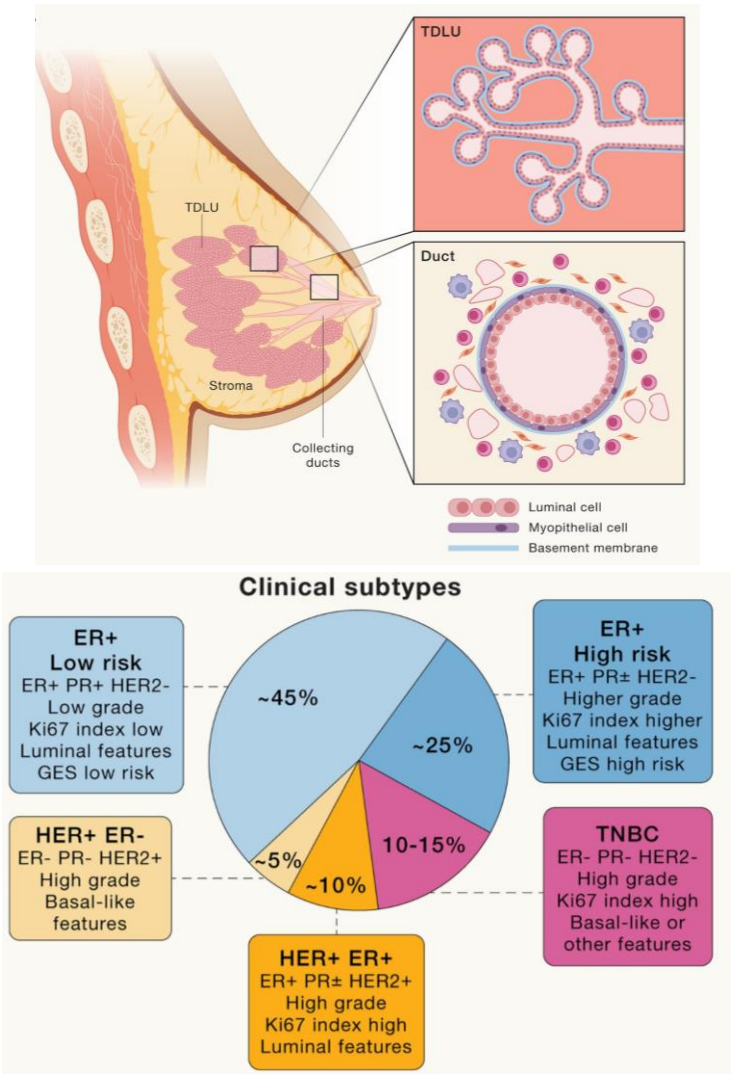

Figure 2.2. In the upper panel, schematic illustration of the human breast, illustrating the terminal ductal lobular unit (TDLU) as the primary functional unit where the majority of tumors originate. Additionally, a cross-sectional view of the branched epithelial ductal tree is presented. In the lower panel, comparison of the primary clinical subtypes of breast cancer is conducted primarily through the examination of histological features and the immunohistochemical expression of key markers, including the estrogen receptor (ER), progesterone receptor (PR), human epidermal growth factor receptor 2 (HER2), and the proliferation marker Ki67[55].

Besides this classification, TNBC appears to be a very highly heterogeneous tumor, characterized by several subtypes which may have different biological behaviors and responses to treatment. In 2021, The Cancer Genome Atlas (TCGA) breast cancer dataset revealed 12 consensus subgroups starting from a normal mammary cell differentiation score analysis, and ordering histologic types into a continuum from stem cell-like to luminal progenitor-like to mature luminal-like[56]. Single-cell transcriptomic analyses have revealed that breast cancer tumors are heterogeneous, even within the same subtype. This means that there are different types of cancer cells within the same tumor, each with its own unique gene expression profile. Breast cancer transcriptome has a wide range of intra-tumoral heterogeneity, which is shaped by the tumor cells and immune cells in the surrounding microenvironment[57,58]. As mentioned above, this heterogeneity has implications for the diagnosis and treatment of breast cancer. It is now clear that tumors cannot be simply classified as one subtype or another. Instead, each tumor must be individually assessed to determine the most appropriate treatment.

The molecular pathways involved in TNBC onset and progression are several, including PI3K-AKT pathway, MAPK signaling pathway, cyclin D1-CDK4/6-RB axis, FGFR pathway but these have a different weight in the frequency of occurrence. Indeed, one of the most frequent pathways found deregulated in TNBC is the PI3K pathway. Different genomic alterations, including activating mutations in PIK3CA, AKT1 or MTOR and inactivating mutations or loss of PTEN, PIK3R1 or INPP4B, can lead to activation of the PI3K pathway. PIK3CA mutations were detected in 7% of TNBC samples from The Cancer Genome Atlas breast cancer dataset and 35% and 30% of samples had additional inactivating alterations in PTEN and INPP4B, respectively. Overall, deregulation of any PI3K pathway component occurs in ~50% of TNBCs[59,60]. Furthermore, even though activating mutations in genes encoding MAPK pathway components (such as KRAS, HRAS, BRAF and MEK1/2) are very rare in TNBC, the amplification of these genes

and non-canonical mechanisms of MAPK pathway activation, including the overexpression of growth factor receptors (such as EGFR, FGFR1 and IGF1R) or loss of negative regulators (including NF1 or DUSP4), have been described and might occur in ~3% of TNBCs[59,61].

The management of early, advanced, and metastatic TNBC has radically shifted over the last few years. Early-stage TNBC is cancer that has not spread beyond the breast or the lymph nodes under the arm. The main treatment for early-stage TNBC is surgery, followed by radiation therapy and chemotherapy (Figure 2.3). Advanced TNBC is cancer that has spread to other parts of the body, such as the lungs, liver, or bones. The main treatment for advanced TNBC is chemotherapy. Other treatments that may be used include targeted therapy and immunotherapy. Metastatic TNBC is cancer that has spread to distant organs and cannot be cured. The goal of treatment for metastatic TNBC is to control the cancer and improve the quality of life. Treatment options for metastatic TNBC include chemotherapy, targeted therapy, immunotherapy, and clinical trials[62].

In this context, important biomarkers with prognostic and predictive utility include the following: BRCA mutation status, PD-L1 immune checkpoint expression, tumor-infiltrating lymphocytes (TIL) content, and somatic genomic signatures indicating homologous recombination deficiency (HRD). BRCA1 (17q21) and BRCA2 (13q12–13) are critical tumor suppressors that serve as guardians of genomic integrity, by promoting high-fidelity HR-mediated repair of double-strand DNA breaks. The cumulative lifetime risk of breast cancer for BRCA1 mutation carriers is 72%, and for BRCA2 mutation carriers, it is 69%. BRCA1 mutation carriers also have an increased risk of ovarian cancer, at 44%, while BRCA2 mutation carriers have an increased risk of ovarian cancer of 17%[63]. BRCA1- and BRCA2-mutated tumors have different molecular, clinical, and histopathological features. BRCA1-mutated tumors are more aggressive, tend to occur earlier in life, and are more likely to be TNBC. BRCA2-

mutated tumors are more likely to be ER+, and are often of the luminal B subtype. TNBC with germline or somatic mutations in BRCA1/2 (about 15%–20%), are sensitive to *synthetic lethality*, which can occur when the loss (mutation and/or inhibition) of two genes essential for cell survival results in cell death, while the loss of either gene alone is not lethal. Only cancer cells carrying gene mutations will be affected. Indeed, in TNBC which display mutations in BRCA1/2 genes synthetic lethality can be triggered by PARP inhibitors that block single-strand DNA repair in the HRD setting. Both olaparib and talazoparib were highly effective in pre-treated patients with a germline mutation[64]. While single-agent PARP inhibitors do not seem to be effective in treating wild-type TNBC, they are being explored for use in combination with immune checkpoint inhibitors (ICIs) in tumors that exhibit "BRCAness" or HRD. The targeting of other DNA damage response proteins, such as selective inhibitors of ATM, ATR, Aurora kinase A, CHK1/2, RAD51, and WEE1, is also being explored, often in combination with PARP inhibitors. Additionally, PD-L1 status of the tumor is also a crucial biomarker to consider when treating TNBC. PD-1 is an immune checkpoint that, when activated by its ligands (PD-L1 and PD-L2), suppresses T cell activity. For advanced TNBC in which the cancer cells have the PD-L1 protein, the first treatment may be immunotherapy (pembrolizumab) with chemotherapy. Indeed, the monoclonal antibody pembrolizumab works by blocking the PD-1 receptor on T cells and releasing the "brakes" on the immune system, allowing T cells to attack cancer cells more effectively. The optimal sequence in patients with PD-L1-positive and germline BRCA1 or BRCA2 mutations would first be checkpoint inhibitor-based therapy and then the PARP inhibitor. For PD-L1 negative and BRCA1 wild-type would rather benefit from sequential single-agent chemotherapy, in which two different drugs are administered in sequence, or combination therapy, in which two drugs are simultaneously given together and might mutually synergize or sensitize their cytotoxic effect on cancer cells.

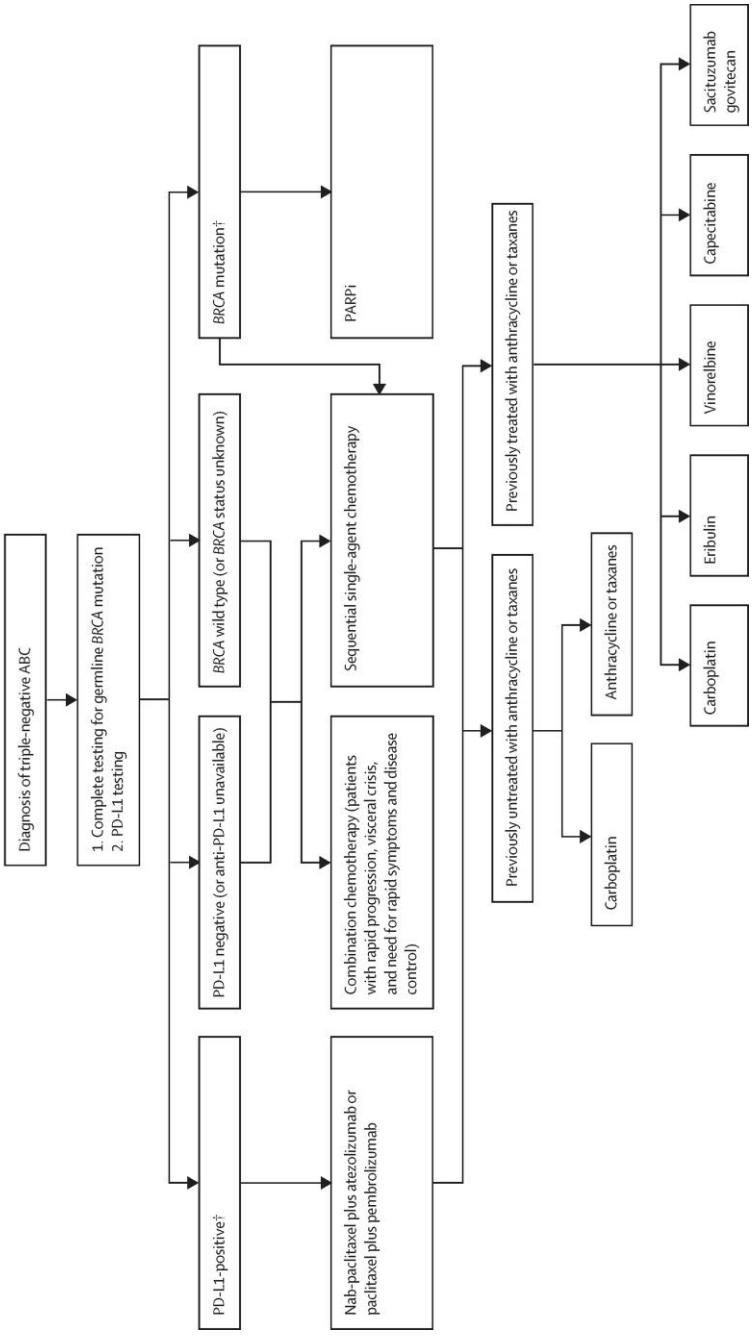

Figure 2.3. Treatment algorithm for triple-negative metastatic breast cancer. ABC=advanced breast cancer. AI=aromatase inhibitor. DFI=disease-free interval. ET=endocrine therapy. PARPi=poly(ADP-ribose) polymerase inhibitor. *Rechallenge with taxanes or anthracycline is possible (if cumulative dose not reached and DFI ≥12 months). †Patients with PD-L1-positive or *BRCA*-mutated breast cancer should first receive a checkpoint inhibitor with taxane, then PARPi (no data available for checkpoint inhibitors as second-line therapy)[65].

Furthermore, anthracyclines (doxorubicin, daunorubicin, epirubicin) and taxanes (paclitaxel, eribulin, vinorelbine) might be used as chemotherapeutic agents in a sequential regimen in the neoadjuvant and adjuvant treatment of early and advanced triple-negative breast cancer both to shrink the tumor volume and to reduce the risk of cancer recurrence. Anthracyclines are drugs acting mainly by intercalating with DNA and inhibiting topoisomerase II enzymes, and creating free radicals that damage DNA, interfering with DNA metabolism and RNA transcription. Taxanes work by interference with microtubules depolymerization during cell division. Standard practice is to administer anthracycline-based chemotherapy followed by a taxane[65]. ADCs (Antibody-Drug Conjugates) represent an emerging therapeutic approach with expanding utilization in advanced-stage breast cancer. ADCs consist of recombinant monoclonal antibodies that are covalently bound to cytotoxic agents via synthetic linkers. Besides direct cytotoxicity, ADCs such as Sacituzumab govitecan can also induce double-strand DNA breaks and enhance the growth inhibitory effect of PARP inhibitors in preclinical models of TNBC, regardless of BRCA1/2 mutational status[66].
Furthermore, it has become increasingly evident that the tumor ecosystem must be considered holistically to understand the biology of breast cancer and improve therapeutic strategies. This is supported by the growing understanding of the co-evolution of tumors and the immune system. A comprehensive view of TNBC as an ecosystem that encompasses the intrinsic and extrinsic features of cancer cells is needed. Indeed, breast carcinoma cells exist within a complex ecosystem comprising diverse cell types that include TILs, fibroblasts, endothelial cells, pericytes, adipocytes, and parenchymal cells. Among these categories, as mentioned above, TILs seem to have the most crucial role in TNBC therapy outcome. They include many types of immune cells infiltrating the tumor with varying density and localization. The most representative are CD8+ T cells, the main effectors of the immune response, CD4+ T helper cells, natural killer cells, M1

macrophages, and dendritic cells (DCs). Stromal and intra-tumoral TILs, easily measured in hematoxylin and eosin (H&E)-stained slides, vary widely within TNBC and their activity in the immune-surveillance are influenced by individual immune cell gene expression, soluble factors such as interferon release, and somatic, epigenetic or germline mutations[54]. Quantitative levels of TILs correlate linearly with lower risk for recurrence or death[67].
Overall, these treatments are the result of years of research into TNBC. However, at the same time, advancing knowledge about this type of tumor suggests the need to develop new therapy strategies that consider the recently discovered characteristics of TNBC.

2.5 m^{6}A in TNBC

The enzymes responsible of the dynamic nature of m^{6}A modification have all been implicated in the regulation of gene expression and the evolution of tumors, including processes like carcinogenesis, metastasis, and progression, particularly in breast cancer. Indeed, m^{6}A methyltransferase METTL3 promotes breast cancer stemness by regulating cell fate determinant SOX2 mRNA, thus influencing the malignant level of ER+ breast cancer[68]. Furthermore, METTL3 increased HBXIP expression forming a positive feedback loop of HBXIP/let-7g/METTL3/HBXIP, leading to accelerated cell proliferation in TNBC. HBXIP-elevated methyltransferase METTL3 promotes the progression of breast cancer via inhibiting tumor suppressor let-7g[69]. Additionally, METTL3 promotes TNBC breast cancer progression via targeting Bcl-2[70] and was also found involved in lung metastasis originating from breast cancer[71]. Finally, METTL3 controls EMT, migration and invasion of TNBC through MALAT1-miR-26b-HMGA2 axis[72].
Less evidence is known about m^{6}A-demethylase FTO, which promotes TNBC progression through inhibiting BNIP3[73].

Moreover, the other m^{6}A-demethylase ALKBH5 regulates NANOG mRNA during hypoxic conditions, inducing TNBC towards stemness[74]. Likewise, it was shown that hypoxia induces the expression of ZNF217, which inhibits METTL3-dependent m^{6}A methylation on NANOG mRNA, thereby promoting the breast cancer stem cell (BCSC) phenotype[75].

M^{6}A readers have also been associated to breast cancer recurrence. Indeed, aberrations of YTHDF1 and YTHDF3 predict poor prognosis in breast cancer patients[76]. Additionally, YTHDF3 induces the translation of m^{6}A-enriched ST6GALNAC5, GJA1, EGFR, VEGFA transcripts to promote breast cancer brain metastasis[77] and promotes autophagy through translation of FOXO3 mRNA[78]. Finally, YTHDF2 reader depletion triggers proteotoxic cell death in MYC-driven TNBC[79]. In summary, m^{6}A modifications play a crucial role in epigenetic regulation, influencing the progression of breast cancer.

These abnormal m^{6}A modifications have a profound impact on the expression, activation, or inhibition of pivotal signaling molecules within critical pathways, as well as on their associated regulatory factors.

In addition, it is worth mentioning the accumulating evidence showing the interplay between m^{6}A and the tumor environment (TME), characterized by hypoxia, aberrant metabolism, immune escape, and chronic inflammation which affect anti-tumor response[80]. Indeed, m^{6}A modification has been reported to remodel TME by regulating the crosstalk between various TME cellular components such as T cell, natural killer cell (NK), dendritic cell (DC), tumor-associated with macrophages (TAM), tumor-associated with fibroblast (TAF), and so on, affecting the anti-tumor immune response[81,82]. This suggests that m^{6}A could serve as a promising target for novel immunotherapies.

2.6 m^{6}A and the DNA damage response

As mentioned above, the treatment of TNBC heavily depends on the induction of DNA damage within cancer cells. In fact, the primary therapeutic approaches for TNBC involve the use of treatments like radiation therapy and chemotherapy, which predominantly consist of DNA-damaging agents. The goal of DNA-damaging agents in cancer treatment is to induce significant and lethal damage to the DNA of rapidly dividing cancer cells. Examples of specific DNA-damaging agents used in cancer therapy include chemotherapy drugs like anthracyclines (e.g., doxorubicin), platinum-based compounds (e.g., cisplatin), alkylating agents (e.g., cyclophosphamide), and topoisomerase inhibitors (e.g., etoposide). Differently from anthracyclines, topoisomerase inhibitors specifically target topoisomerase enzymes (type I or type II), preventing the enzyme from resealing the DNA break created to relieve torsional stress and facilitating DNA unwinding and manipulation during DNA replication and transcription. As result, DNA-damage inducers accumulation of DSBs leads to the activation of DNA damage response pathways. The DNA damage response (DDR) is a complex network of signaling pathways that coordinate cellular responses to various types of DNA damage. It involves a series of sensors, transducers, mediators, and effectors to detect and repair damaged DNA or induce cell cycle arrest and apoptosis when necessary.
Two key kinases acting upstream in the DDR are ATM (Ataxia Telangiectasia Mutated) and ATR (Ataxia Telangiectasia and Rad3-related)[83]. In detail, sensors recognize DNA damage and initiate the DDR cascade. Examples include the MRE11-RAD50-NBS1 (MRN) complex, which senses double-strand breaks (DSBs) and activates the transducer kinase ATM, and the RPA protein which detects single-strand breaks (SSB) and activates the ATRIP-ATR complex, which senses single-stranded DNA (ssDNA) regions. ATR and Chk1 (checkpoint kinase 1) are crucial for the S and G2 checkpoints, whereas ATM-Chk2 functions from G1 to G2

phases, promoting p53 and p21 expression. Furthermore, once activated, ATM catalyzes the phosphorylation (γ) of H2AX, which accumulates forming nuclear foci to DSBs and serves as an amplifier of DNA damage.

Mediator proteins relay the signal from the transducers to the downstream effectors. Notable mediators include MDC1 (Mediator of DNA Damage Checkpoint 1) and 53BP1 (p53-binding protein 1). Effectors are proteins that execute various DDR functions, such as DNA repair, cell cycle arrest, or apoptosis. Effector proteins like BRCA1, RAD51, and PARP play pivotal roles in DNA repair. BRCA1 promotes homologous recombination (HR) repair of DSBs. RAD51 facilitates strand exchange during HR. PARP (Poly ADP-ribose Polymerase) is involved in DNA repair, particularly in base excision repair (BER) and single-strand break repair (SSBR). Upon binding to damaged DNA, PARP becomes activated and catalyzes the formation of poly ADP-ribose (PAR) chains on itself and other target proteins. These PAR chains serve as a signal to recruit DNA repair proteins to the site of damage[84].

Notably, m^6A modification can be induced by UV irradiation and recruited to UV-damaged sites to promote DNA repair and cellular resistance to UV damage. Indeed, DNA polymerase κ (Pol κ), which has been implicated in both nucleotide excision repair and trans-lesion synthesis, required the catalytic activity of METTL3 for immediate localization to ultraviolet-induced DNA damage sites[85].

m^6A can also occurs at the RNA strand of R-loops, which are RNA:DNA hybrid that can potentially induce DNA damage and genomic instability when they persist or are not properly resolved by RNAseH. Depletion of METTL3 promotes the accumulation of R-loops, leading to DSBs in iPSCs suggesting that m^6A prevents the formation of R-loops and DNA damage in iPSCs[86]. Furthermore, phosphorylation-dependent activation of METTL3 by ATM at serine 43 results in m^6A methylation of DNA damage-associated ncRNAs, which are recognized and protected by

YTHDC1, leading to the recruitment of BRCA1 and RAD51 for HR-mediated DSBs repair[87].
In addition, FTO KO promotes the accumulation of DSBs in mouse osteoblasts induced by DNA-damaging agents and the metabolic stress, high-fat diet while it decreases the level of Hspa1a and Kdm2a protein that is associated with DNA repair[88].
METTL3 augments m^6A on EGF transcript, which is recognized and stabilized by YTHDC1, resulting in elevated RAD51 expression and enhanced HR efficacy[89].
Finally, data on YTHDF1 show its positive regulation of HR-related factors RAD51 and BRCA1, in a METTL14-dependent manner[90]. All this evidence agrees with the protective role of m^6A modification on DNA integrity.

2.7 STM2457: inhibition of m^6A as therapeutic target

METTL3 is primarily associated with oncogenic functions in both hematological malignancies and solid tumors. In many instances, METTL3 oncogenic roles are closely tied to its m^6A methyltransferase activity. In fact, the overexpression of wild-type METTL3 has been shown to promote the growth of acute myeloid leukemia (AML) cells, whereas METTL3 lacking catalytic activity does not exhibit this effect[91]. This underscores the importance of METTL3 m^6A methyltransferase function. Specifically, METTL3 promotes leukemogenesis by increasing the stability and/or translation of key mRNAs, including MYC, BCL2, PTEN, SP1, and SP2, in an m^6A-dependent manner[91,92]. Additionally, METTL3 can also act as an m^6A reader, enhancing the translation of its target mRNAs, such as EGFR, TAZ, BRD4, and CD9 transcripts in lung adenocarcinoma (LUAD) progression[93]. The underlying mechanism involves METTL3 binding simultaneously to the m^6A-modified 3' UTR of its target mRNAs and eIF3H, which is in close proximity to the 5' cap of mRNAs. This binding event induces

mRNA circularization, facilitating ribosome recycling and thereby accelerating translation.
However, recently METTL3 has been reported to have a similar role in promoting the translation of non-m^{6}A-modified epigenetic factor mRNAs in gastric cancer. In this context, METTL3 binds to polyadenylate-binding protein 1 (PABPC1), stabilizing its interaction with the 5' cap-binding complex eIF4F[94]. It's noteworthy that METTL3, which is primarily a nuclear protein, exhibits cytoplasmic mislocalization in various malignancies, including LUAD, gastric cancer, and myeloid leukemia[95,96]. This suggests that METTL3 functions beyond its enzymatic activity, such as its role in translation promotion, might be still unknown. Given the oncogenic nature of METTL3, approaches to study its function at the molecular level and in terms of phenotypic effects include METTL3 depletion/inhibition by RNA interference and chemical inhibition.
The advantages of using inhibitory molecules are multiple. Some inhibitory molecules can have greater stability over time compared to RNA molecules, which can degrade rapidly inside cells. This can be advantageous in long-term applications. RNA interference can potentially cause off-target interference, unintentionally inhibiting similar but non-targeted genes, while inhibitory molecules can reduce this risk due to their specific design. More importantly, inhibitor compounds may have a higher likelihood of reaching their targets within cells and tissues *in vivo*, as they are not subject to the same cellular barriers that RNA can encounter. This renders these molecules more readily commercializable and accessible compared to the complex technologies of RNA interference.
To date, strategies employed to reduce METTL3 activity include the inhibition of the enzyme catalytic domain, which transfer a methyl group from SAM to the adenosine, or targeting non-active sites of METTL3 through allosteric inhibition by disrupting the METTL3–METTL14 complex, which is essential for METTL3 m^{6}A deposition.

Previous studies on nucleotide-based molecules which showed low cellular permeability and poor selectivity led to the development of the first METTL3 inhibitor by Caflisch's group, named UZH1a[97]. It was developed through a structure-based drug design approach and showed selectivity over a panel of other SAM-dependent methyltransferases (DOT1L, G9a, MLL4, PRDM9, PRMT1, SETD2, and SMYD3). Additional optimization of the compound led to the synthesis of UZH2[98], which represented the first single-digit nanomolar METTL3 inhibitor (IC_{50} = 0.005 μM) being highly cell-permeable and relatively stable. Although results indicated no significant changes in the m^1A/A and m^7G/G ratios (which are deposited by TRMT6 and guanine-7 methyltransferase RNMT, respectively), following 6 days of incubation at 10 μM, data have not proven exclusive selectivity towards METTL3 methyltransferases, meaning the compound might inhibit other SAM-dependent methyltransferases[99].
In 2021, STORM Therapeutics leaded by Kouzarides started with a high throughput screening (HTS) of 250.000 compounds and led to the identification of the inhibitor STM2457[100], with *in vitro* and *in vivo* optimized pharmacokinetics. Differently from UZH2, STM2457 exhibited over 1000-fold METTL3 selectivity over a panel of 45 RNA, DNA, and protein methyltransferases as well as 468 kinases. It was also tested in a panel of various AML cell lines, where it impaired cell proliferation with IC_{50} values of 0.7-10.3 μM, induced cell cycle arrest, myeloid differentiation, and triggered apoptosis. Subsequent studies in patient-derived xenograft (PDX) mouse models showed that daily treatment with 50 mg/kg of STM2457 led to impairment of engraftment and AML expansion *in vivo* and significantly prolonged the mouse lifespan. Moreover, the anti-leukaemic effect was also confirmed by the reduction of human CD45+ cells in the bone marrow and spleen following treatment, along with no significant weight variations and toxicity. Re-transplantation experiments in rodents using murine or patient-derived AML cells from primary transplants treated with STM2457 demonstrated a prolongation of survival and

an evident decrease of AML cells in peripheral blood[99,100]. Latest evidence showed that pharmacological inhibition of METTL3 impacts specific hematopoietic lineages, particularly on erythroid differentiation and maturation[101].
Recently, STORM Therapeutics announced its lead clinical candidate for METTL3 inhibition, named as STC-15, which is currently in Phase 1 clinical trial in patients with solid tumors[102]. In summary, STM2457 represents a groundbreaking proof of concept that the inhibition of an RNA methyltransferase through small molecules can be efficacious in treating cancer.

3. AIMS

N^6-methyladenosine (m^6A) is the most abundant internal modification in mRNA and plays a crucial role in RNA metabolism. The enzyme Methyltransferase-like 3 (METTL3) catalyzes m^6A methylation on mRNA molecules. METTL3 has been found to be upregulated in different types of cancer, where it plays a crucial role in cancer progression, metastasis, and drug resistance.

The inhibition of METTL3 by a small molecule, STM2457, has shown promising antitumor activity in acute myeloid leukemia (AML). However, the specific cancer types in which METTL3 inhibitors may be most effective remain to be determined. In breast cancer, several studies have reported that METTL3 knockdown resulted in marked suppression of proliferation, invasiveness, and metastasis. Thus, METTL3 inhibition has been proposed as a promising therapeutic approach for breast cancer.

Triple-negative breast cancer (TNBC) is the most aggressive subtype of breast cancer, with a poor prognosis, high risk of recurrence, and limited treatment options. Conventional chemotherapy and DNA-damaging agents are the mainstays of treatment for this cancer. Remarkably, METTL3 is recruited to DNA damaged sites and is required for subsequent DNA repair. METTL3 knockdown decreases DNA repair activity and sensitize cancer cells to genotoxic drugs. TNBC is characterized by high level of METTL3, and its nuclear catalytic activity correlates with invasiveness and metastasis.

Therefore, this study investigates catalytic inhibition of METTL3 by STM2457 could be a valuable treatment option for TNBC. The specific aims of this thesis are:

1. Investigation of the effects of m^6A depletion by METTL3 methyltransferase chemical inhibition (METTL3i).
2. Identification of the pathways affected by METTL3i.
3. Evaluation of combination therapy with METTL3i to target TNBC *in vitro* and *in vivo*.

4. RESULTS

4.1 METTL3 levels are upregulated in TNBC cell lines

METTL3 methyltransferase is known to be upregulated in BC tissues at both the RNA and protein levels. Here, we evaluated METTL3 protein levels in TNBC cell lines (MDA-MB-231, MDA-MB-468, HCC1395, MDA-MB-436, HCC1937) and detected a significant increase in METTL3 protein levels in TNBC compared to MCF-10A cell line (Figure 4.1), which represents the counterpart normal cell line isolated from a human mammary gland.

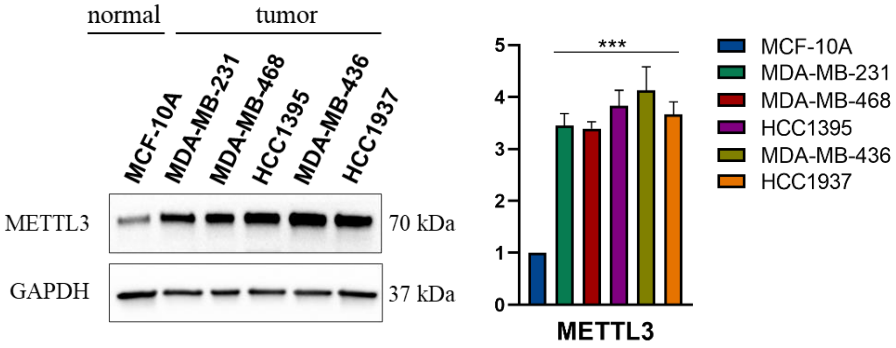

Figure 4.1. Left panel, representative Western blot showing METTL3 protein levels in different TNBC cell lines; right panel, METTL3 protein levels densitometric analysis on five independent biological replicates. Data on the histogram are shown as mean ± s.d.. Statistical analysis was performed on GraphPad software by using unpaired two-tailed Student's t-test, *** $p < 0.001$.

Notably, despite the different nature of the above mentioned TNBC cell lines, METTL3 protein levels are coherently upregulated in these cells, even though they share a different mutational genetic background and therefore belong to different subtypes (according to Lehmann's classification[54], Table 1). Moreover, their multiple histological and molecular characteristics have important implications for therapy.

TNBC cell line	Morphology	Histology	Tumor source	Mutant gene
MDA-MB-231	MSL	Adenocarcinoma	Metastasis (pleural effusion)	$BRAF^{+/-}$, $CDKN2A^{homo}$, $KRAS^{+/-}$, $NF2^{homo}$, $TP53^{homo}$
MDA-MB-468	BL1	Adenocarcinoma	Metastasis (pleural effusion)	$PTEN^{homo}$, $RB1^{homo}$, $SMAD4^{homo}$, $TP53^{homo}$
HCC1395	Unclassified	Primary ductal carcinoma	Primary	$BRCA1^{homo}$, $CDKN2A^{homo}$, $PTEN^{homo}$, $TP53^{homo}$
MDA-MB-436	MSL	Adenocarcinoma	Metastasis (pleural effusion)	$BRCA1^{homo}$, $RB1^{homo}$
HCC1937	BL1	Primary ductal carcinoma	Primary	$BRCA1^{homo}$, $TP53^{homo}$

Table 1. Table shows histological and molecular characteristics of the TNBC cell lines used in this work, based on Lehmann's classification[54]: basal-like A (BL1), mesenchymal stem-like (MSL).

4.2 METTL3 chemical inhibition reduces TNBC cell proliferation and viability

To estimate the oncogenic role of m^6A in TNBC, we employed chemical inhibition of the m^6A methyltransferase METTL3. By taking advantage of the recently identified METTL3 methyltransferase inhibitor STM2457[98], we treated TNBC cell lines with different concentrations (μmol/L) of STM2457. Cell proliferation and viability assays performed after treatment with

STM2457 showed a significant effect on all TNBC cell lines, in reducing cell number and viability at increasing concentrations. To assess the safety of STM2457 treatment we also treated MCF10A healthy cell line to exclude its potential toxic side effects. Notably, MCF-10A viability was not substantially reduced by STM2457 treatment, maintaining around 70% of viability at the highest concentration and time of administration of the drug (Figure 4.3).

(A)

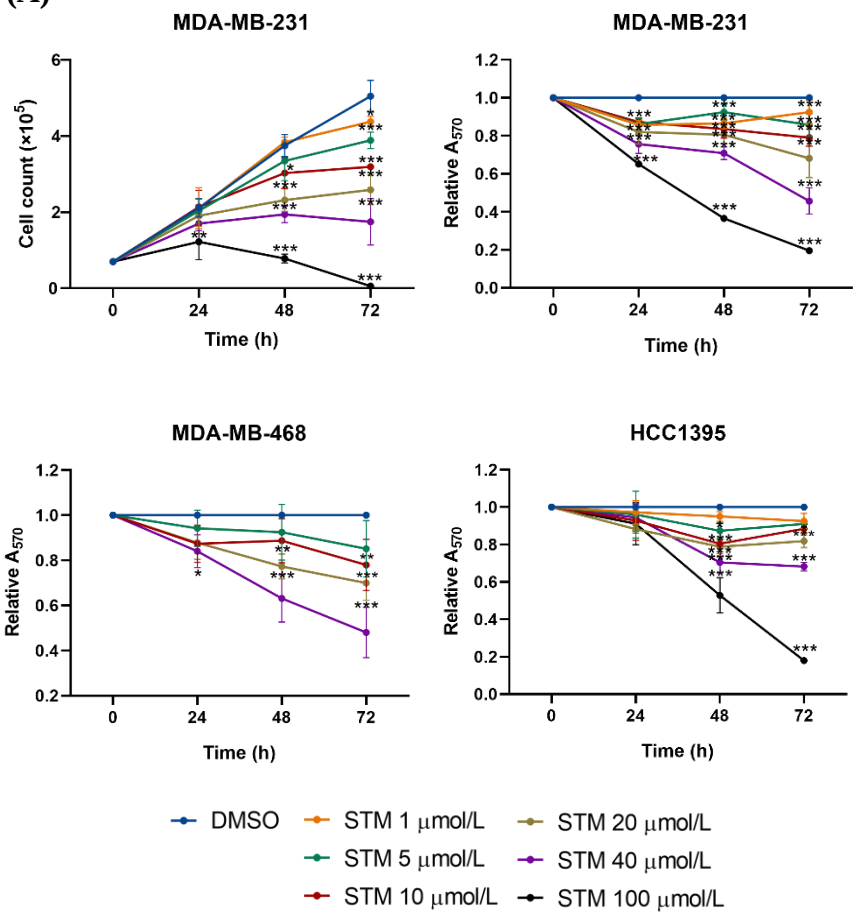

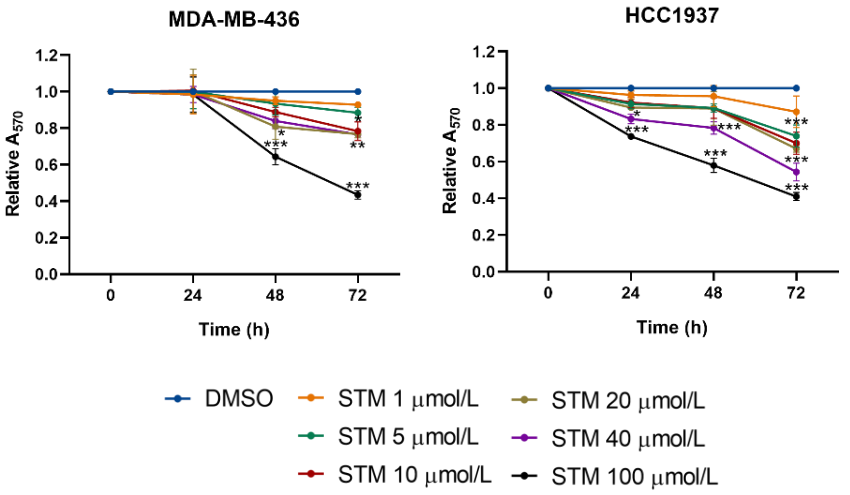
MDA-MB-436
HCC1937
Relative A570
Time (h)
DMSO
STM 1 µmol/L
STM 5 µmol/L
STM 10 µmol/L
STM 20 µmol/L
STM 40 µmol/L
STM 100 µmol/L

(B)

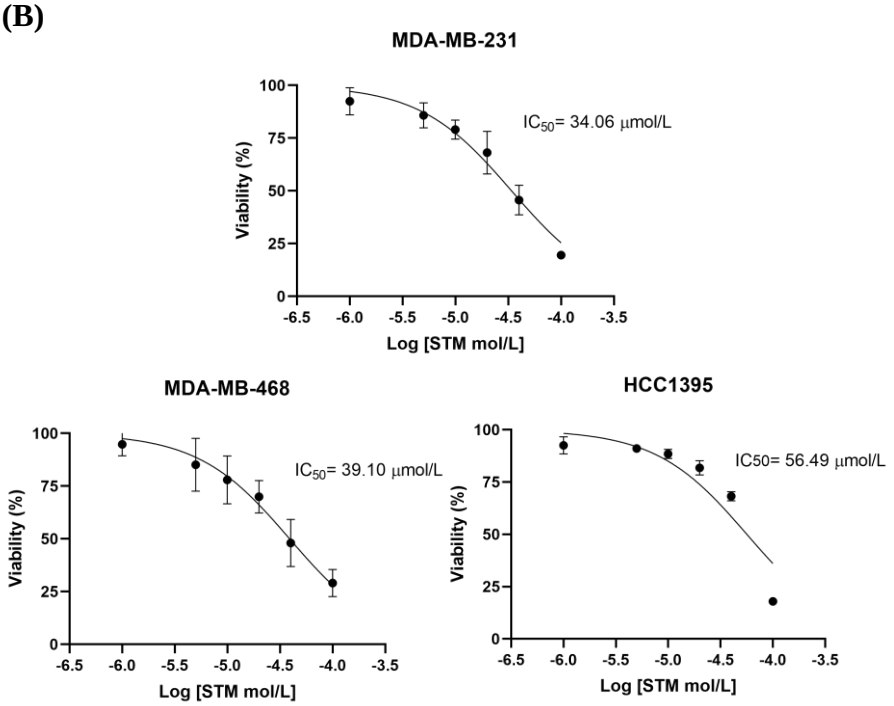
MDA-MB-231
IC50= 34.06 µmol/L
MDA-MB-468
IC50= 39.10 µmol/L
HCC1395
IC50= 56.49 µmol/L
Viability (%)
Log [STM mol/L]

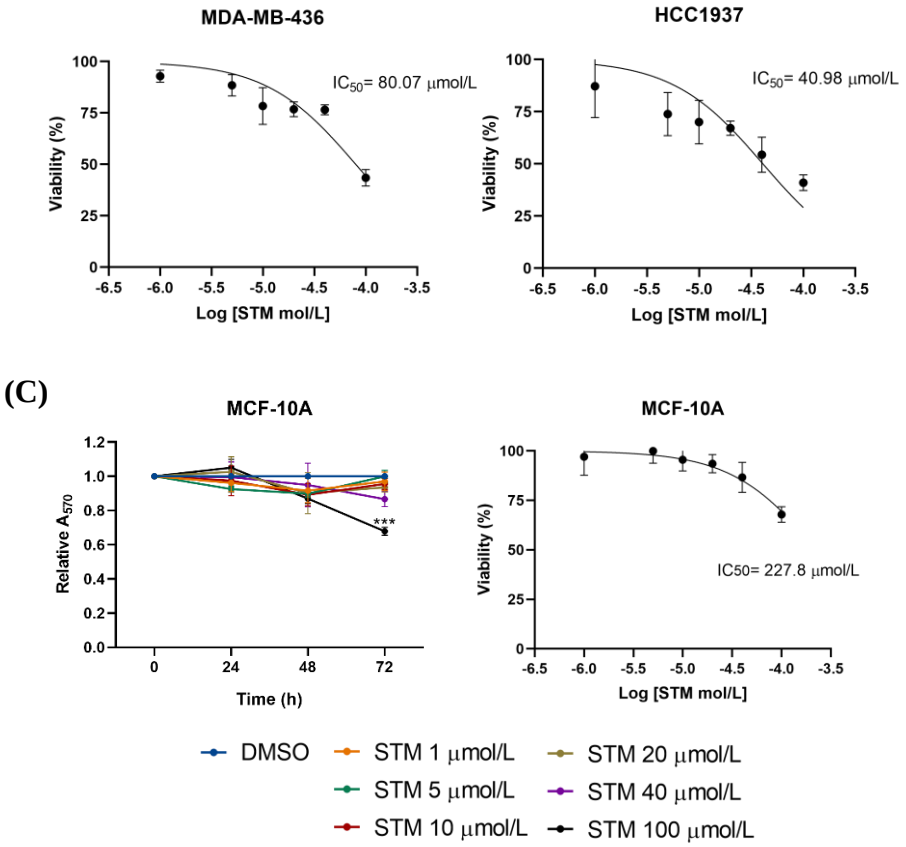

Figure 4.2. (A) Growth curve and MTT assays of TNBC cell lines treated with different concentrations of STM2457 (STM) (1 µmol/L, 5 µmol/L, 10 µmol/L, 20 µmol/L, 40 µmol/L, 100 µmol/L) or DMSO for 72h. (B) Corresponding IC_{50} graphs calculated at 72h of STM treatment for all TNBC cell lines. (C) MTT assay and IC_{50} of MCF-10A, exposed to STM for 72h. For MTT assays, DMSO viability was set to a value of 1 and STM-induced viability absorbance values were compared to DMSO absorbance. Statistical analyses were performed on GraphPad software, by using two-way ANOVA Dunnett's multiple comparisons test * $p<0.05$, ** $p<0.01$, *** $p<0.001$, $p<0.0001$. Values are shown as mean ± s.d. All experiments were performed on three independent biological replicates.

4.3 METTL3 chemical inhibition reduces TNBC cell colony formation and cell migration

To better characterize the effect of STM2457 treatment on TNBC cells, we analyzed whether STM2457 can alter TNBC cell colony formation, which is the ability of a single cell to grow into a colony, providing insights into various aspects of cellular behavior and biology. Indeed, cell colony formation assay performed on TNBC cells and MCF-10A cell line treated with 5 µmol/L of STM2457 showed a strong effect on the reduction of the number of colonies, only in TNBC cell lines and not the corresponding healthy line (Figure 4.3).

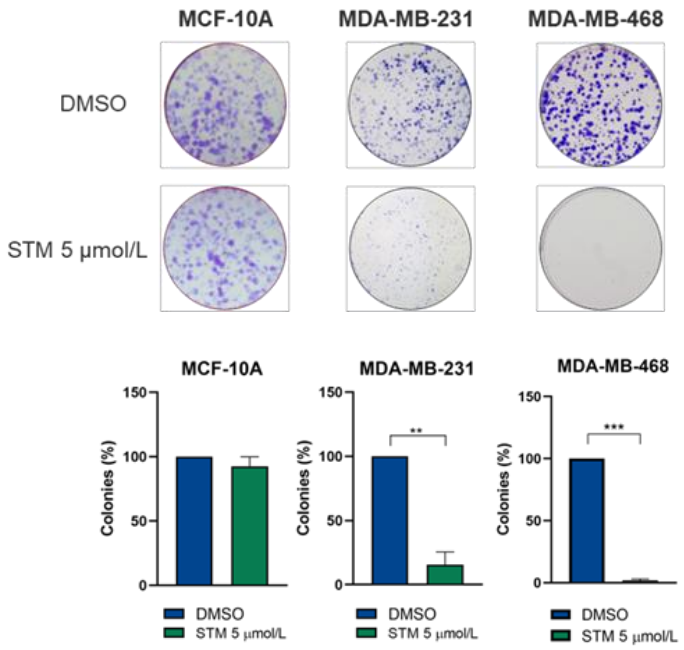

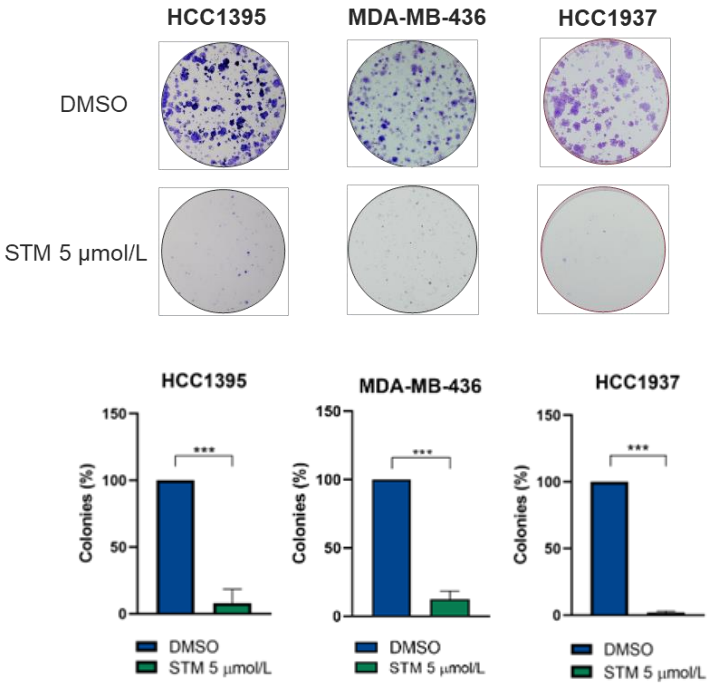

Figure 4.3. Cell colony formation assay of TNBC (MDA-MB-231, MDA-MB-468, HCC1395, MDA-MB-436, HCC1937) and MCF-10A cell lines treated with 5 µmol/L of STM2457 (STM) or DMSO every 72 hours. Colonies were fixed in methanol and stained with crystal violet (0.5% crystal violet, 20% methanol). Histograms indicate the percentage of colonies from three independent replicates. Statistical analyses were performed on GraphPad software, by using unpaired two-tailed Student's t-test *** $p<0.001$, $p<0.0001$.

We next proceeded to assess if STM2457 treatment can influence TNBC cell migration *in vitro* by performing wound healing assay on MDA-MB-231 cells. Treatment with STM2457 significantly reduced TNBC migration as indicated by the inability of the treated cells to efficiently close the gap in the cell monolayer (Figure 4.4).

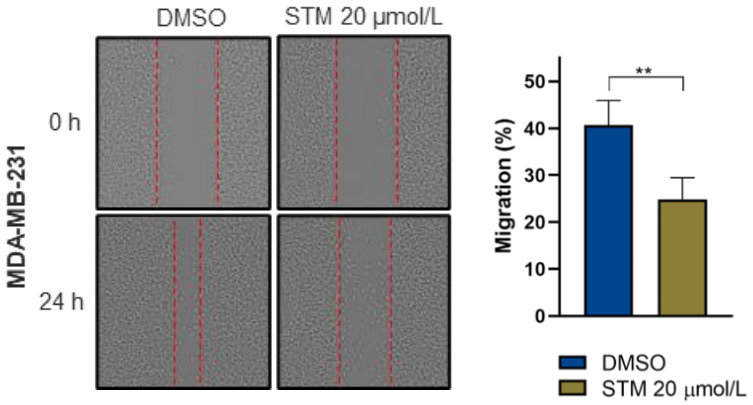

Figure 4.4. Wound healing assay upon STM2457 (STM) treatment shows a substantial reduction of TNBC migration ability in MDA-MB-231 cells. Scratch was performed in the middle of the cell monolayer prior to treatment with DMSO and STM in FBS-free DMEM medium, to avoid cell proliferation bias. Wound closure was followed up to 24h and wound areas were measured with ImageJ software. The histogram represents migration evaluation from three independent experiments. Statistical analyses were performed on GraphPad software, by using unpaired two-tailed Student's t-test ** $p<0.01$. Values are shown as mean ± s.d.

Since MDA-MB-231 cell line is widely recognized to be one of the most aggressive and invasive cells among other TNBC cell lines, the aforementioned experiment and the ones that will follow were performed on MDA-MB-231 cells, as its aggressive and invasive properties make it a valuable model for studying cancer metastasis and exploring potential therapeutic approaches.
Taken together, these data indicate that METTL3 catalytic activity sustains TNBC proliferation, migration, and metastatic potential.

4.4 Chemical inhibition by STM2457 is specific for METTL3 methyltransferase

To ensure that the phenotype observed so far on TNBC was due to the modulation of m^6A modification, we performed METTL3 knockdown and compared STM2457-induced phenotype with TNBC cells silenced for METTL3. We transduced MDA-MB-231 cells with lentiviral particles carrying Tet-On doxycycline-inducible shRNAs against METTL3. Thus, we measured METTL3 protein levels to verify METTL3 knockdown efficacy by performing Western Blot analysis. Growth curve of MDA-MB-231 cell lines treated with two different shRNAs against METTL3 (shMETTL3#1 and shMETTL3#2) or scramble shRNA (shSCR) was performed after 96h of doxycycline administration (Figure 4.5). METTL3 knockdown with both shRNAs significantly reduced MDA-MB-231 cell proliferation. Specificity of the effects of STM2457 on TNBC cells was also confirmed by colony formation assay and would healing assay upon METTL3 knockdown. Overall, these data confirmed that the action of STM2457 inhibitor is due to its inhibition of METTL3 methyltransferase activity.

.

(A)

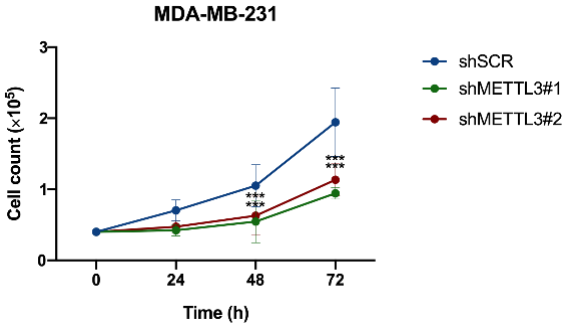
MDA-MB-231
Cell count (×10⁵)
3
2
1
0
0
24
48
72
Time (h)
***
***
***
***
shSCR
shMETTL3#1
shMETTL3#2

(B)

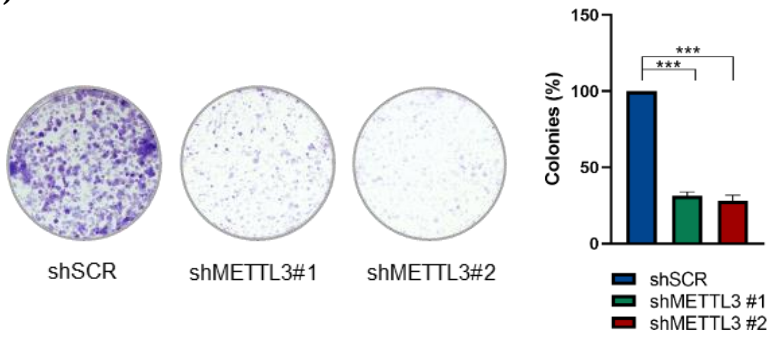
shSCR
shMETTL3#1
shMETTL3#2
Colonies (%)
150
100
50
0
***
***
shSCR
shMETTL3 #1
shMETTL3 #2

(C)

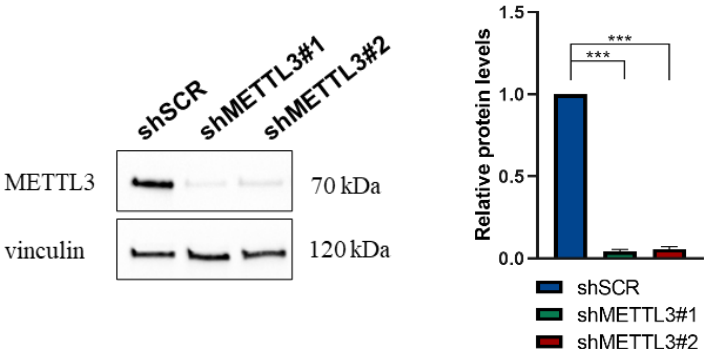
shSCR
shMETTL3#1
shMETTL3#2
METTL3
70 kDa
vinculin
120 kDa
Relative protein levels
1.5
1.0
0.5
0.0
***
***
shSCR
shMETTL3#1
shMETTL3#2

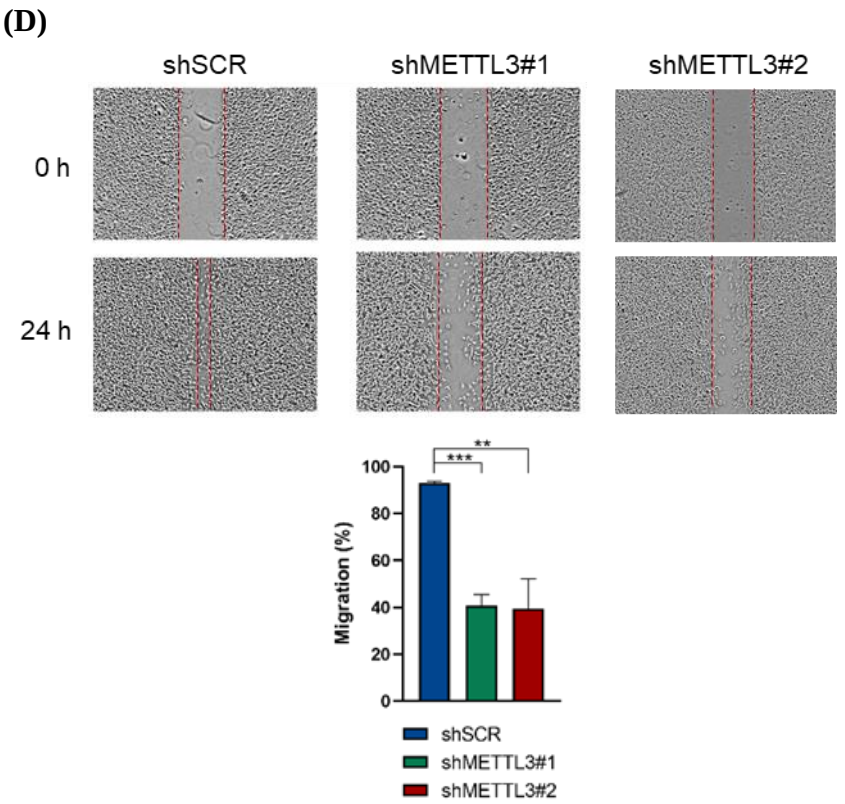

Figure 4.5. (A) Growth curve of MDA-MB-231 cell lines treated with two different shRNAs against METTL3 (shMETTL3#1 and shMETTL3#2) or scramble shRNA (SCR). (B) Cell colony formation assay of MDA-MB-231 cell lines upon METTL3 knockdown. (C) Representative Western Blot indicating the drop of METTL3 protein levels upon METTL3 knockdown in MDA-MB-231 cells. Protein levels were analyzed 96h after shRNAs-induction by doxycycline administration. (D) Migration evaluation ability through wound healing assay of MDA-MB-231 cells treated upon METTL3 knockdown. Statistical analyses were performed on GraphPad software, by using one-way ANOVA Dunnett's multiple comparisons test for the growth curve, and unpaired two-tailed Student's t-test for densitometric and migration analysis *** $p<0.001$, $p<0.0001$. Values are shown as mean ± s.d. All experiments were performed on three independent biological replicates.

4.5 STM2457 treatment reduces m^{6}A globally and specifically on mRNAs

Prior to proceeding in the exploration of the effects of METTL3 inhibition on TNBC, m^{6}A levels upon STM2457 treatment were assessed. The efficacy of the chemical inhibition of METTL3 was determined through the evaluation of m^{6}A abundancy in the cells, after STM2457 administration. M^{6}A levels were analyzed both globally and specifically on messenger RNAs. For the former aim, a colorimetric assay was performed in MDA-MB-231 cells upon 48 hours of STM2457 treatment. To avoid the background signal of m^{6}A on ribosomal RNA (rRNA) (deposited by METTL5 methyltransferase), total RNA extraction was followed by polyA$^+$ RNA purification (messenger RNAs) to remove rRNA. m^{6}A levels were measured after a sufficient period of time (48 hours) for a complete turnover of mRNAs to observe a significant change in mRNA profiles. Indeed, upon STM2457 treatment, m^{6}A levels were globally reduced (Figure 4.6).

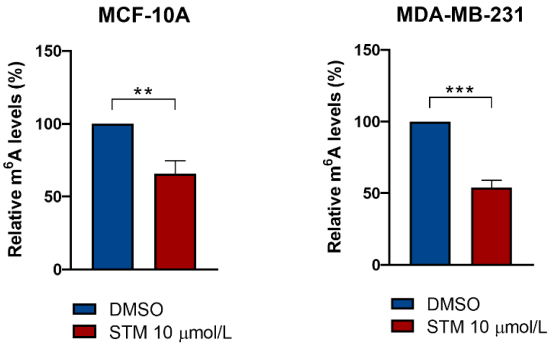

Figure 4.6. Histogram showing global m^{6}A levels reduction after 10 µmol/L of STM2457 (STM) treatment for 48h in MCF-10A and MDA-MB-231 cells. Epiquik colorimetric assay was used to determine the relative quantification of m^{6}A RNA methylation status of the two different RNA samples from three independent biological replicates: DMSO absorbance was set to a value of 1 and STM-treated poliA$^+$-mRNAs sample was compared to DMSO. Statistical

analyses were performed on GraphPad software, by using unpaired Student's t-test, *** $p<0.001$. Values are shown as mean ± s.d.

To validate the information regarding the global decrease in m^6A levels, we also performed MeRIP (m^6A-IP) experiment followed by RT-qPCR on specific RNAs that are commonly known to be targets of METTL3 methyltransferase. Evidence by MeRIP-sequencing (m^6A-seq) experiments obtained from GEO database (GSE183014)[103] performed in MDA-MB-231 cells showed enrichment of m^6A modification in several mRNAs. Among those, MYC and BiP mRNAs were found to be highly m^6A-methylated. We confirmed the decrease of m^6A levels as a consequence of METTL3 inhibition on both MYC and BiP mRNAs. Indeed, the percentage of m^6A-methylated transcripts was significantly reduced upon STM2457 treatment (Figure 4.7).

(A)

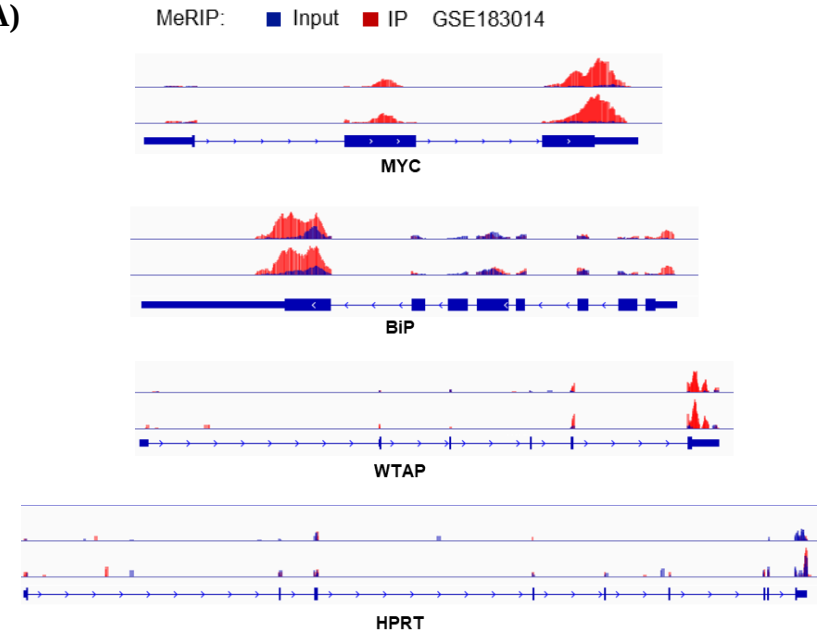

(B)

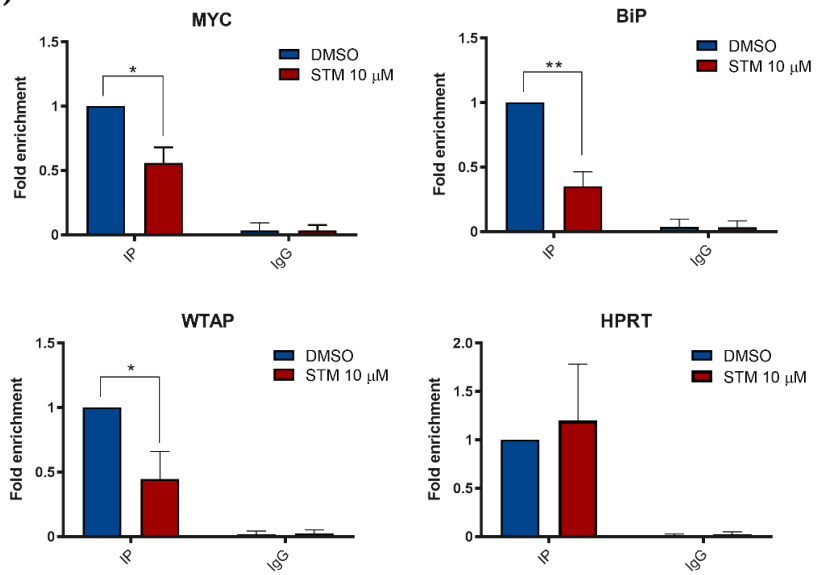

Figure 4.7. (A) Integrative genomics viewer (IGV) plots of m^{6}A abundance in MYC, BiP, WTAP and HPRT transcripts in MDA-MB-231. Data were obtained from GEO GSE183014, showing the differential enrichment peaks of m^{6}A modification of MYC and BiP transcripts in IP samples (blue) over the input (red). (B) qPCR analysis of m^{6}A Immunoprecipitation (IP) in individual transcripts in MDA-MB-231 cells treated with DMSO and 10 μmol/L STM2457 (STM). Relative ratio (fold enrichment) obtained in the presence of DMSO was set to 1. Positive control as highly m^{6}A-methylated transcript (WTAP) and negative control as non-m^{6}A-methylated transcript (HPRT) are also shown in the figure. Statistical analyses were performed on GraphPad software, by using unpaired Student's t-test * $p<0.05$, ** $p<0.01$. Values are shown as mean ± s.d. from three independent biological replicates.

4.6 RNA-sequencing and MeRIP-seq show differential gene expression upon METTL3 chemical inhibition

To gain insights into the molecular and cellular processes involved in response to STM2457 treatment, we performed RNA-sequencing analysis of MDA-MB-231 TNBC cells treated with 10 µmol/L of STM2457 for 48 hours. We found 3182 downregulated and 3237 upregulated genes. Gene ontology analysis of differentially expressed genes showed a significant downregulation of biological processes involved in cell proliferation, translation, and DNA repair (Figure 4.8). This result agrees with that of previous analyses performed upon METTL3 knockdown in breast cancer cells[88] and, above all, upon inhibition of METTL3 by STM2457 in AML cell lines[99]. Thus, these data indicate that genes involved in fundamental processes and, notably, DNA repair are significantly affected in MDA-MB-231 cells inhibited for METTL3.

(A)

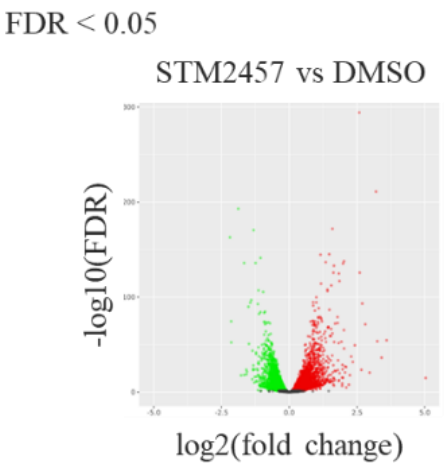

(B)

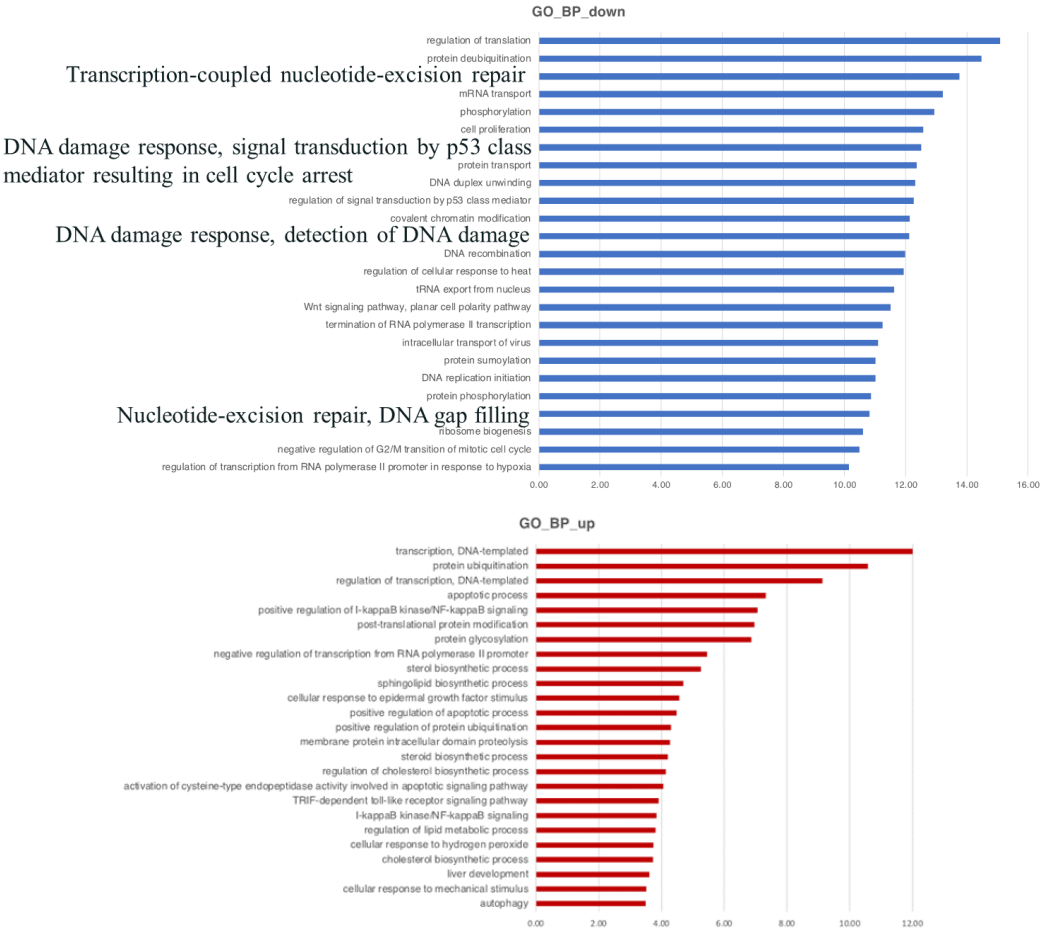

Figure 4.8. (A) The Volcano plot shows the relationship between the fold-change and the significance of the differential expression test for each gene in the genome in STM2457 vs DMSO-treated MDA-MB-231 cells. Black dots represent the genes that are not significantly differentially expressed, while red and green dots are the genes that are significantly up- and down-regulated, respectively. (B) The significant GO terms associated with biological processes of differentially expressed genes are shown. Biological processes involved in DNA damage response and DNA repair are highlighted.

To test whether the altered gene expression could be a consequence of the inhibition of m^{6}A modification, we crossed RNA-seq analysis with the m^{6}A distribution on the transcriptome to identify the genes that were both differentially expressed and m^{6}A-mehylated. Comparison of RNA-seq analysis with MeRIP-seq dataset performed in MDA-MB-231 cells[103] indicated a substantial overlap in differentially expressed genes and m^{6}A-methylated mRNAs (Figure 4.9). Gene Ontology biological process ontology was used to identify the most represented gene functions. Indeed, the analysis of differentially expressed genes that contain m^{6}A marks showed a significant downregulation of biological processes associated with cell cycle and DNA damage. We focused on DNA damage since it has been identified as a significant pathway regulated by METTL3 and is relevant to TNBC therapy.

(A)

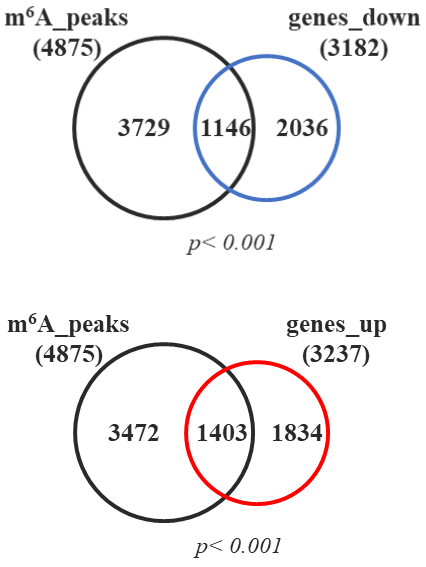

(B)

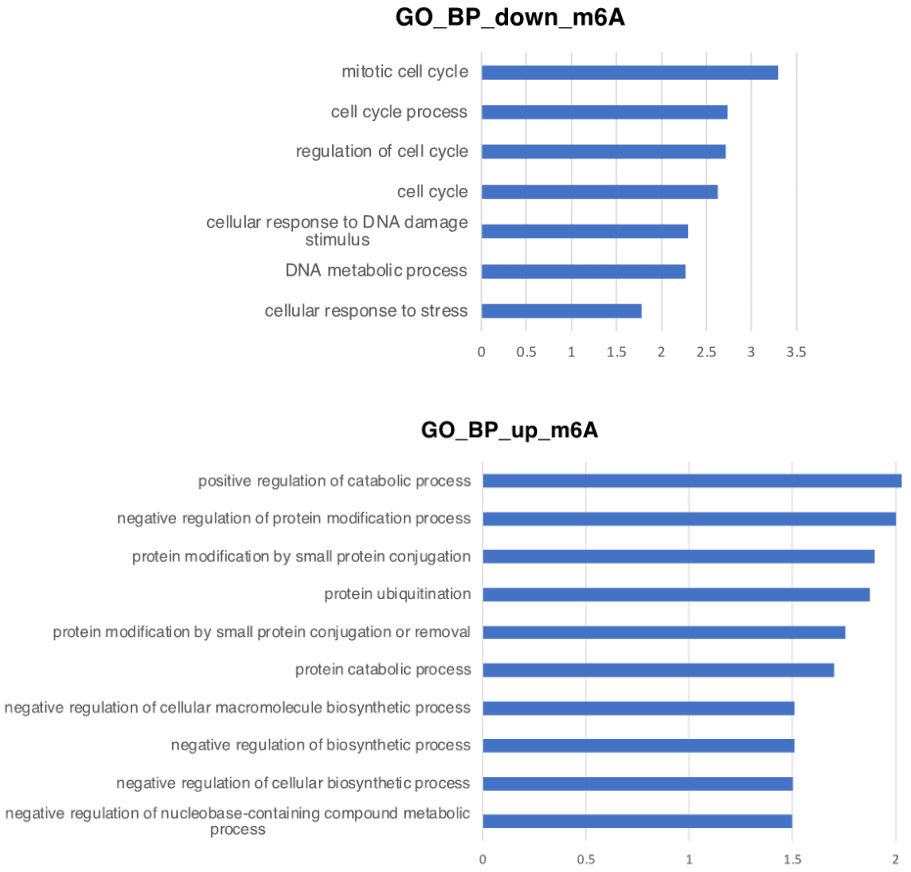

Figure 4.9. (A) Overlap between differentially regulated and m^{6}A methylated genes. Hypergeometric analysis indicated that the correlation is highly significant. (B) Enrichment analysis based on the GO biological process ontology was used to identify the most represented gene functions in m^{6}A-marked genes that were found down- (upper panel) or up- (lower panel) regulated in the RNA-seq.

4.7 STM2457 treatment affects the DNA damage response

Since first-line chemotherapy for TNBC is represented, above all, by DNA damage inducers, we were interested in exploring the connection between m^{6}A and DNA damage. Evidence indicates the involvement of m^{6}A writer METTL3 and m^{6}A reader YTHDF1 in DNA damage repair in many tumors, including breast cancer[89]. Thus, we examined DNA damage potential induction following treatment with STM2457 by measuring γ-H2AX, phosphorylated form of histone variant H2AX which marks DNA damage. Furthermore, to investigate whether DNA damage was due to a direct or indirect by STM2457, we assessed BRCA1, a well-established tumor suppressor involved in HR (Homologous Recombination) repair, and RAD51, which facilitates strand exchange during HR. Notably, we observed decreased BRCA1 and RAD51 protein levels and a concomitant increase of γ-H2AX protein levels, suggesting an inactivating role of m^{6}A modification in the DDR (DNA damage response) (Figure 4.10). These findings are in line with the RNA-seq results, which report the downregulation of genes involved in the DNA damage response.

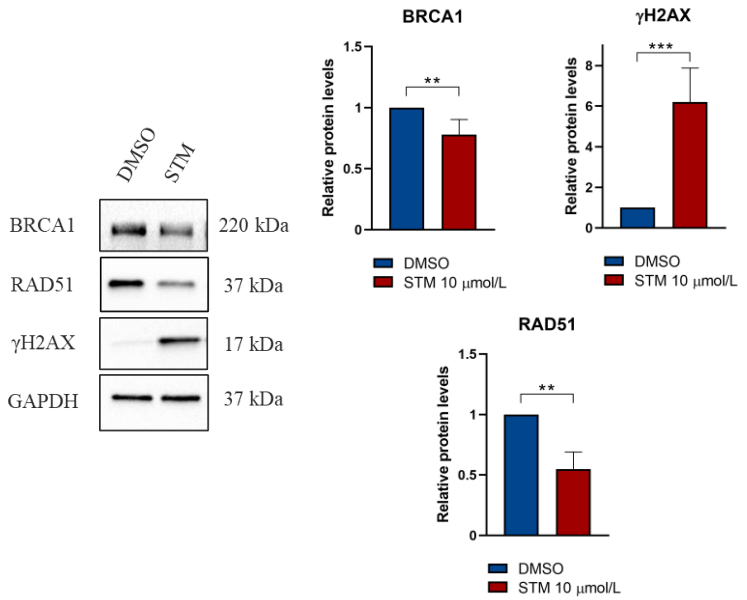

Figure 4.10. Representative Western blot showing BRCA1, γ-H2AX and RAD51 protein levels following 10 μmol/L STM2457 treatment for 72h in MDA-MB-231 cells. The histograms show the densitometric analysis on five independent biological replicates. Statistical analyses were performed on GraphPad software, by using unpaired two-tailed Student's t-test ** $p<0.01$, *** $p<0.001$. Values are shown as mean ± s.d.

To verify the m^6A-dependency of the effect observed, DNA damage induction was also evaluated upon knockdown of METTL3 methyltransferase, which was already known to influence DNA repair (Figure 4.11).

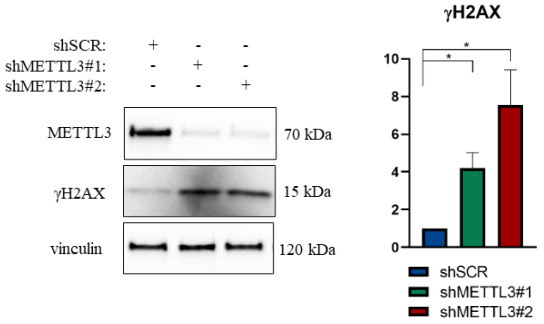

Figure 4.11. Representative Western blot of γH2AX levels in MDA-MB-231 interfered for METTL3; histogram represents densitometric analysis of γH2AX/vinculin ratio from three independent experiments. Statistical analyses were performed on GraphPad software, by using one-way ANOVA Tukey's multiple comparisons test. Values are shown as mean ± s.d.

It is important to emphasize that MDA-MB-231 cells are BRCA1/2 wild type. Even though BRCA1 expression levels are not consistently altered if not slightly downregulated in the RNA-seq analysis performed on STM2457-treated cells, BRCA1 might be post-transcriptionally regulated by YTHDF1[89] or by other mechanisms, potentially both direct and indirect, through which m^6A modification might act on the DNA damage response.

4.8 Combined treatment of STM2457 and DNA-damaging agents impairs MDA-MB-231 survival

Given the array of benefits associated with combined chemotherapy[104], especially within highly heterogeneous tumors as in TNBC, we investigated the effect of METTL3 inhibition in combination with DNA-damaging therapy. Among DNA-damaging agents, platinum-based chemotherapeutics, and PARP inhibitors, such as olaparib (Lynparza), mostly showed favorable responses in TNBC with BRCA1/2 mutations[65]. Thus, we examined the effect of METTL3 inhibition on the response to cisplatin (CDDP) and the PARP1/2 inhibitor olaparib in MDA-MB-231 cell line. By carrying wild-type BRCA1/2 gene, MDA-MB-231 cells are characterized by lower sensitivity to DNA damaging agents. With the aim of enhancing treatment efficacy while minimizing unwanted side effects and resistance issues, we used STM2457 (IC_{50} 34 μmol/L), cisplatin and olaparib below the IC_{50} for combined treatment. Notably, we observed a strong reduction of MDA-MB-231 cell proliferation and viability (Figure 4.12).

(A)

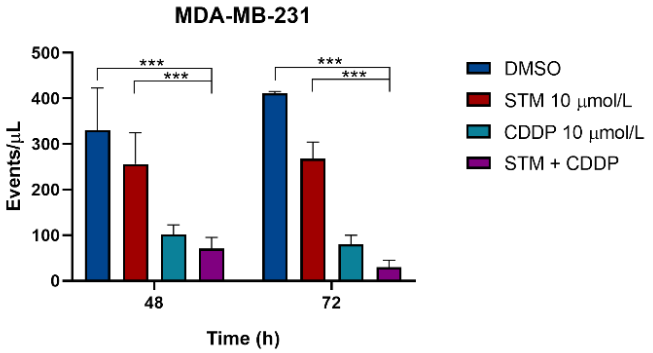

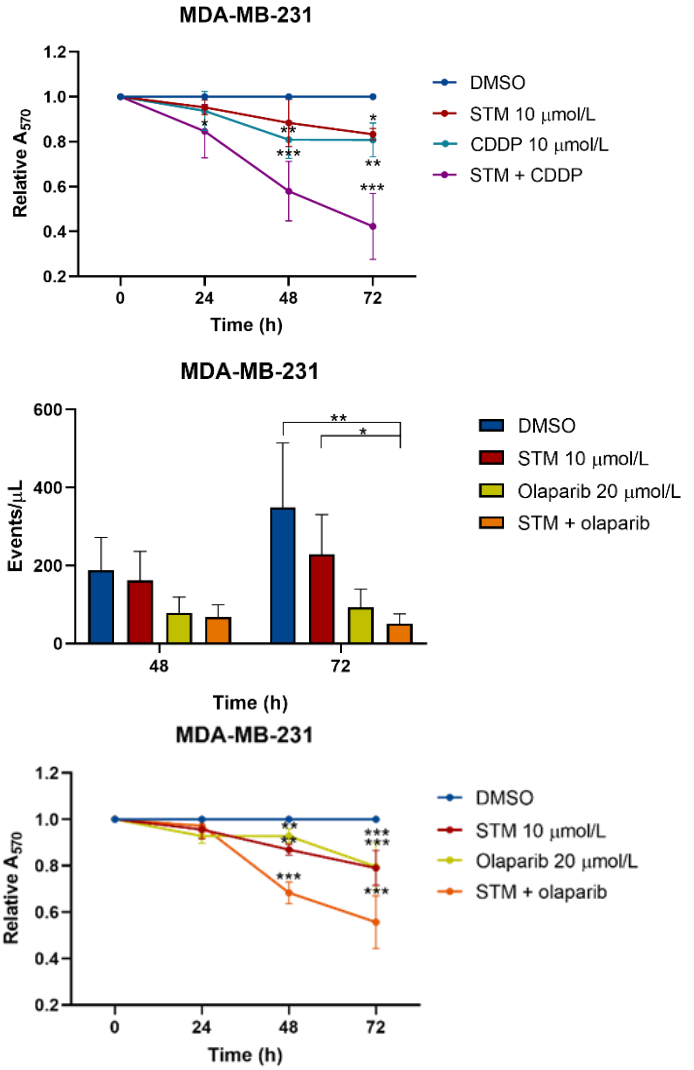

Figure 4.12. Cell count (events/µL) using flow cytometry and MTT assay of MDA-MB-231 cells treated A) with STM2457 (STM) 10 µmol/L, cisplatin (CDDP) 10 µmol/L or combination of both drugs, and B) with STM 10 µmol/L, olaparib 20 µmol/L or combination of both drugs. DMSO viability was set to a value of 1 and STM-induced viability absorbance values were compared to DMSO absorbance. Statistical analyses were performed on GraphPad software, by using two-way ANOVA Dunnett's multiple comparisons test for MTT assays and cell count (events/µL) analysis * $p<0.05$, ** $p<0.01$, *** $p<0.001$,

p<0.0001. Values are shown as mean ± s.d. All experiments were performed on three independent biological replicates.

To get a deeper understanding of the decrease in cell number and viability, we conducted flow cytometry analysis to assess the apoptotic rate subsequent to STM2457 treatment. Remarkably, the inhibition of cell growth and decreased cell viability were accompanied by higher apoptosis rate when STM2457 was combined with both cisplatin and olaparib, alternatively, as compared to cells treated with the single drugs (Figure 4.13).

(A)

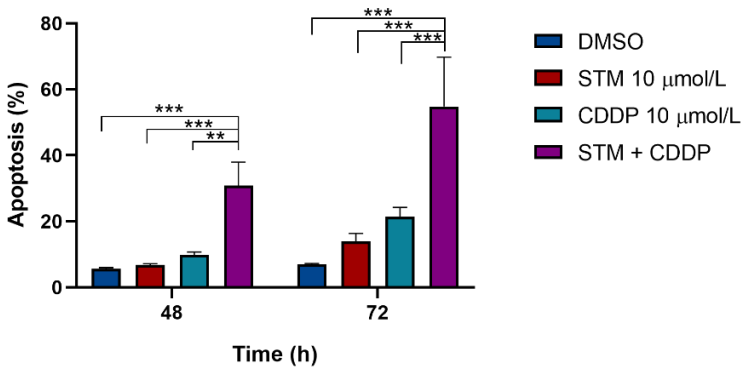

(B)

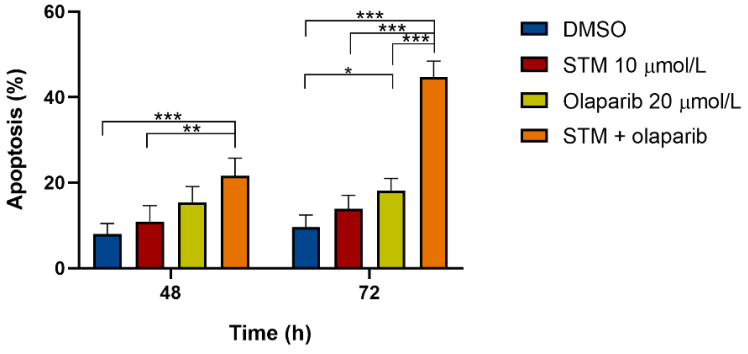

(C)

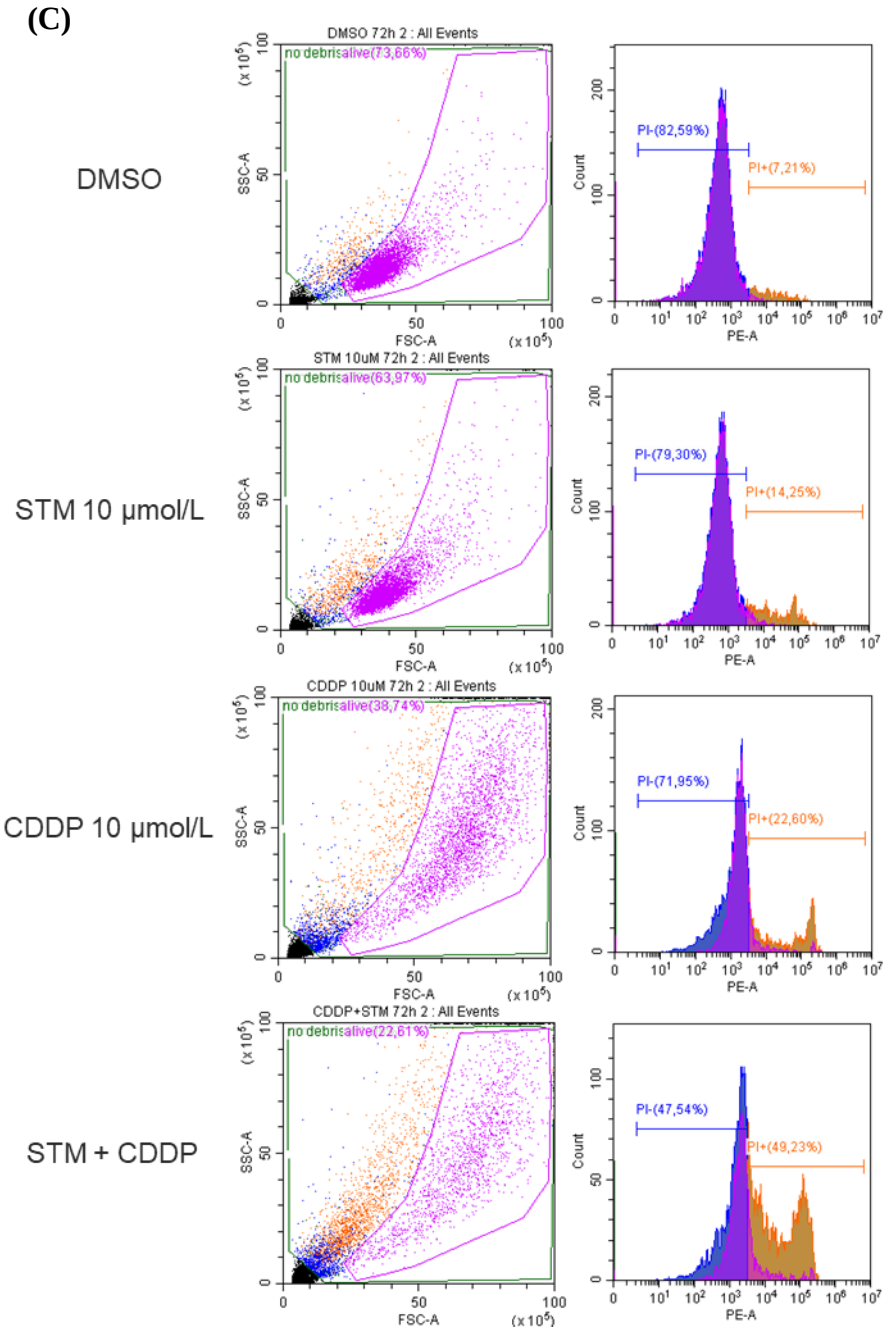
DMSO
DMSO 72h 2 : All Events
no debrisative(73,66%)
PI-(82,59%)
PI+(7,21%)
STM 10 µmol/L
STM 10uM 72h 2 : All Events
no debrisative(63,97%)
PI-(79,30%)
PI+(14,25%)
CDDP 10 µmol/L
CDDP 10uM 72h 2 : All Events
no debrisative(38,74%)
PI-(71,95%)
PI+(22,60%)
STM + CDDP
CDDP+STM 72h 2 : All Events
no debrisative(22,61%)
PI-(47,54%)
PI+(49,23%)
SSC-A
FSC-A
PE-A
Count

(D)

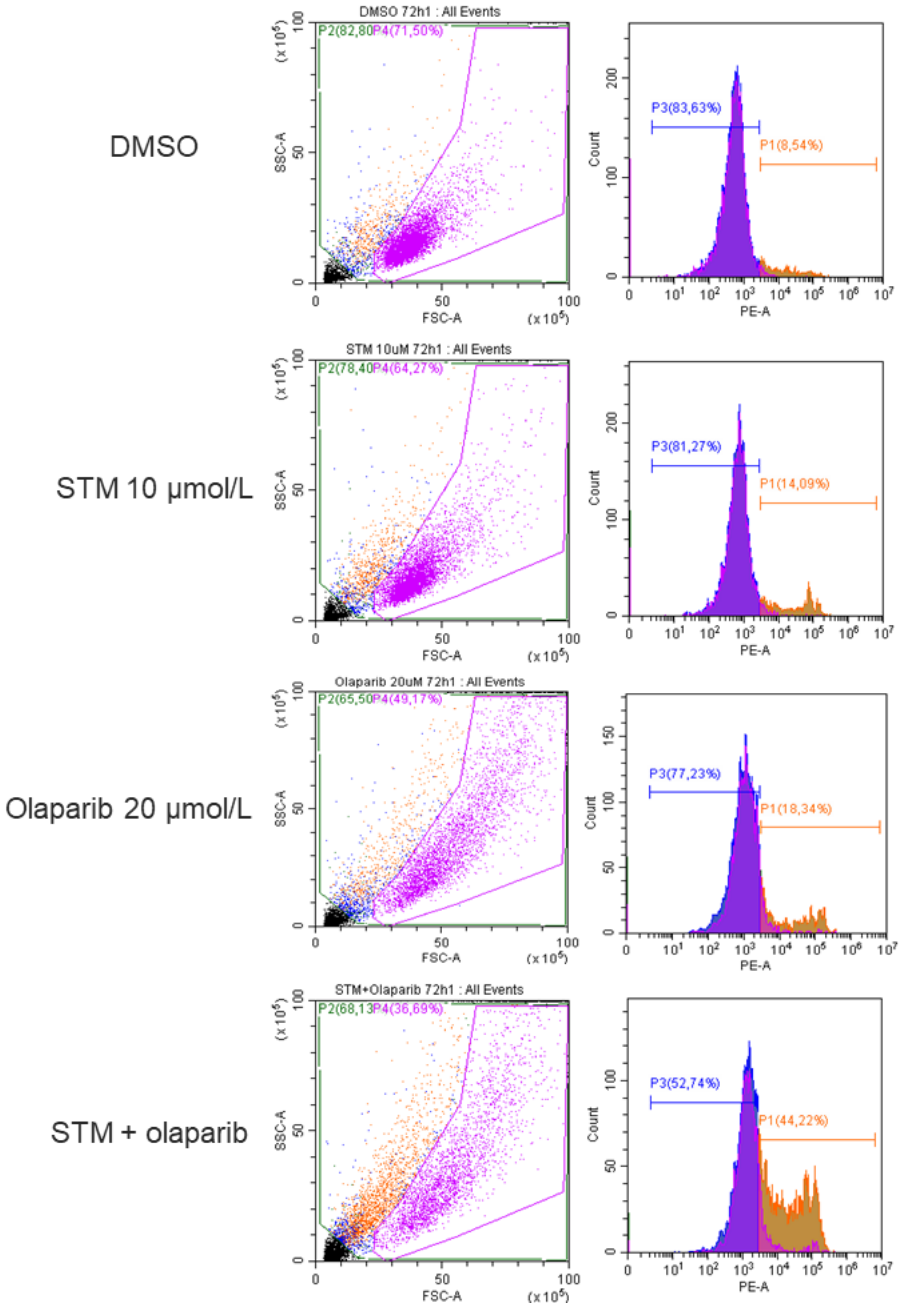
DMSO
DMSO 72h1 : All Events
P2(82,80P4(71,50%)
P3(83,63%)
P1(8,54%)
STM 10 µmol/L
STM 10uM 72h1 : All Events
P2(78,40P4(64,27%)
P3(81,27%)
P1(14,09%)
Olaparib 20 µmol/L
Olaparib 20uM 72h1 : All Events
P2(65,50P4(49,17%)
P3(77,23%)
P1(18,34%)
STM + olaparib
STM+Olaparib 72h1 : All Events
P2(68,13P4(36,69%)
P3(52,74%)
P1(44,22%)
SSC-A
FSC-A
Count
PE-A

Figure 4.13. (A) Histogram represents the percentage of apoptotic cells treated with STM 10 μmol/L, CDDP 10 μmol/L or combination of both drugs in MDA-MB-231 cells. Representative scatter plot showing cell population and percentage of propidium iodide (PI) positive cells. (B) Histogram represents the percentage of apoptotic cells treated with STM 10 μmol/L, olaparib 20 μmol/L or combination of both drugs in MDA-MB-231 cells. (C, D) Representative scatter plot showing cell population and the percentage of propidium iodide (PI) positive cells. Statistical analyses were performed on GraphPad software, by using two-way ANOVA Tukey's multiple comparisons test for the apoptotic rate (% PI^+) analysis * $p<0.05$, ** $p<0.01$, *** $p<0.001$, $p<0.0001$. Values are shown as mean ± s.d. All experiments were performed on three independent biological replicates.

Consistently, the level of phosphorylation of the histone variant H2AX (γH2AX) was significantly increased in combined treatments with the METTL3 catalytic inhibitor in respect to single drug treatments. Notably, we observed diminished RAD51 foci to DNA following treatment with STM2457, upon damage induced by cisplatin and olaparib, alternatively, indicating impairment of the DNA damage response pathway (Figure 4.14).

(A)

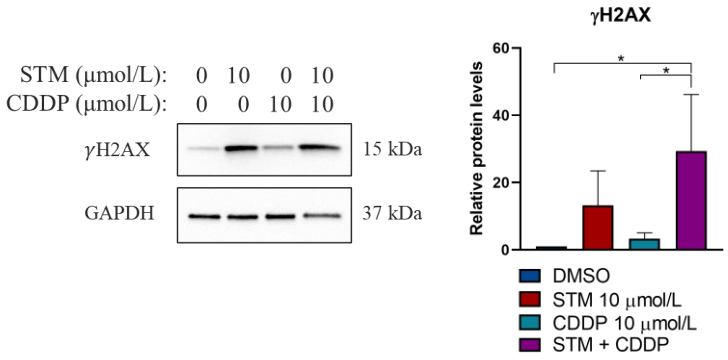

(B)

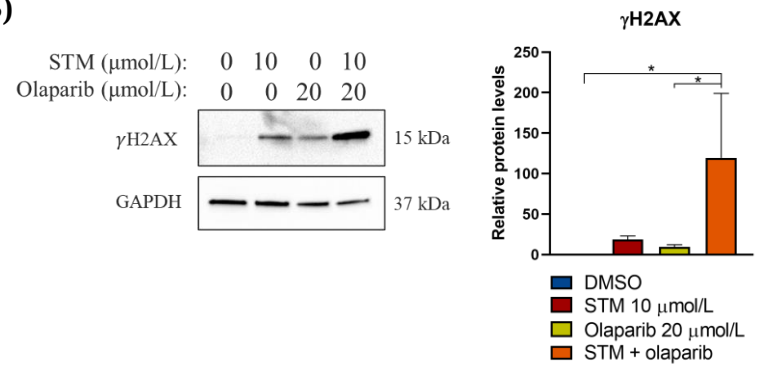
STM (μmol/L): 0 10 0 10
Olaparib (μmol/L): 0 0 20 20
γH2AX
15 kDa
GAPDH
37 kDa
γH2AX
Relative protein levels
250
200
150
100
50
0
*
*
DMSO
STM 10 μmol/L
Olaparib 20 μmol/L
STM + olaparib

(C)

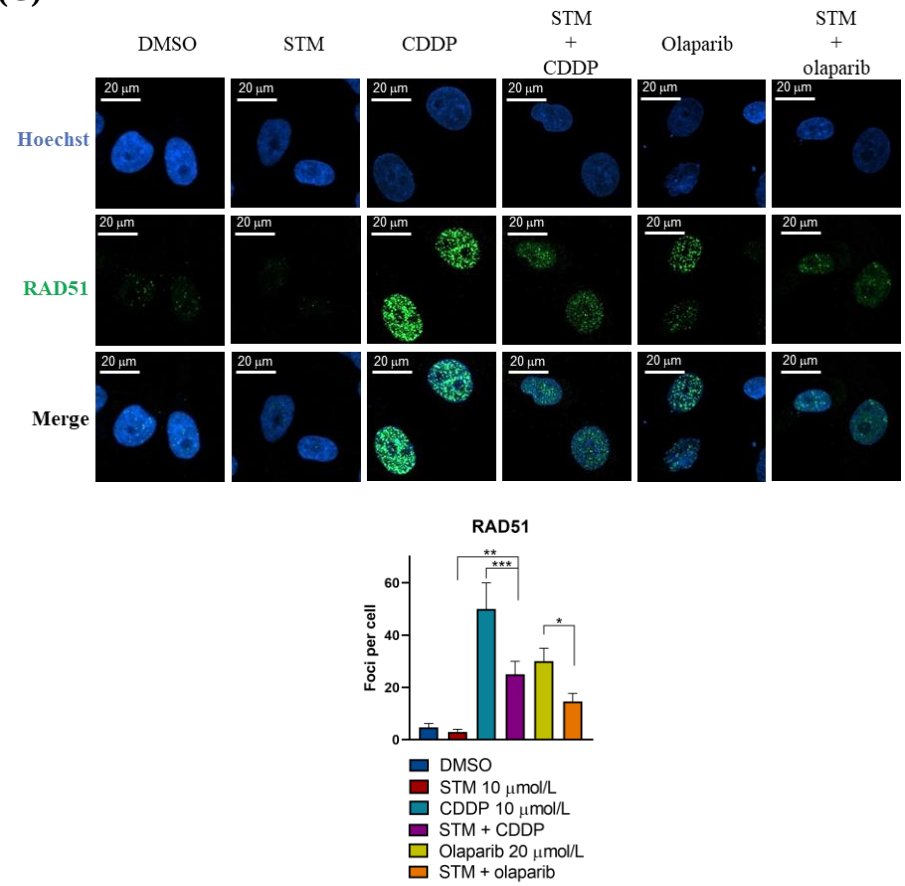
DMSO
STM
CDDP
STM + CDDP
Olaparib
STM + olaparib
Hoechst
RAD51
Merge
20 μm
RAD51
Foci per cell
60
40
20
0
**
***
*
DMSO
STM 10 μmol/L
CDDP 10 μmol/L
STM + CDDP
Olaparib 20 μmol/L
STM + olaparib

Figure 4.14. (A) Representative Western blot of γH2AX levels in MDA-MB-231 cells treated with STM 10 μmol/L, CDDP 10 μmol/L or combination of both drugs; the histogram represents densitometric analysis of γH2AX/GAPDH ratio from three independent experiments. (B) Representative Western blot of γH2AX levels in MDA-MB-231 cells treated with treated with STM 10 μmol/L, olaparib 20 μmol/L or combination of both drugs; the histogram represents densitometric analysis of γH2AX/GAPDH ratio from three independent experiments. (C) Immunofluorescence analysis of RAD51 foci number in MDA-MB-231 cells treated with treated with STM 10 μmol/L, CDDP 10 μmol/L, olaparib 20 μmol/L or combination of both drugs, alternatively; *n*=50 cells were calculated in each group Statistical analyses were performed on GraphPad software, by using one-way ANOVA Tukey's multiple comparisons test * $p<0.05$, ** $p<0.01$, *** $p<0.001$, $p<0.0001$. Values are shown as mean ± s.d

Altogether, these data indicate that STM2457 enhances the response of TNBC cells to DNA damage-inducing therapies and, more importantly, strongly sensitizes TNBC cells carrying wild-type BRCA1/2 to DNA damage induced by genotoxic chemotherapy or PARP inhibition.

4.9 STM2457 inhibitor affects metastatic potential *in vivo* in zebrafish

Until now in this research, the effects of m^6A modification inhibition have been investigated solely *in vitro* using cellular systems of TNBC. To gain a more comprehensive understanding of STM2457 impact, we additionally considered the complexity of a *in vivo* environment. After observing the decrease in cell migration caused by STM2457, we proceeded to examine its impact on cancer cell metastasis. We selected the highly metastatic MDA-MB-231 TNBC cell line for injection in zebrafish larvae, a

well-established xenograft model for the study of cancer cell motility and metastasis *in vivo*[105]. In order to follow MDA-MB-231 cells throughout the Zebrafish larva, we first generated MDA-MB-231 GFP+ stable cell line. In this regard, we cloned eGFP into a transposable vector (ePB-PGK-BSD plasmid) to obtain MDA-MB-231 cells which constitutively express GFP fluorescent protein (Figure 4.15).

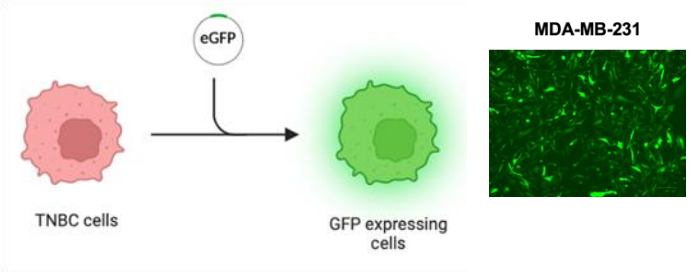

Figure 4.15. Representative illustration of MDA-MB-231 transfected cells for ePB-PGK-BSD containing eGFP construct. The image on the right shows MDA-MB-231 cells stably expressing GFP fluorescent protein. Illustration was created on BioRender tool.

MDA-MB-231 GFP+ cells were microinjected into the perivitelline space of 48 hours post-fertilization (hpf) embryos and the xenografts were incubated with each drug or combinations of them at the same concentrations selected for the *in vitro* assays. Although some extravasated cells were scattered throughout the larva, the caudal haematopoietic tissue (CHT) region was the most affected by the presence of GFP-positive clusters, thus micrometastasis were quantified in this region. Interestingly, while each drug displayed the ability to decrease the metastatic activity of the cells when administered alone, we documented the clear tendency of the combined STM2457+CDDP and STM2457+olaparib treatments to synergize, causing the drop in the number/size of micrometastasis (Figure 4.16).

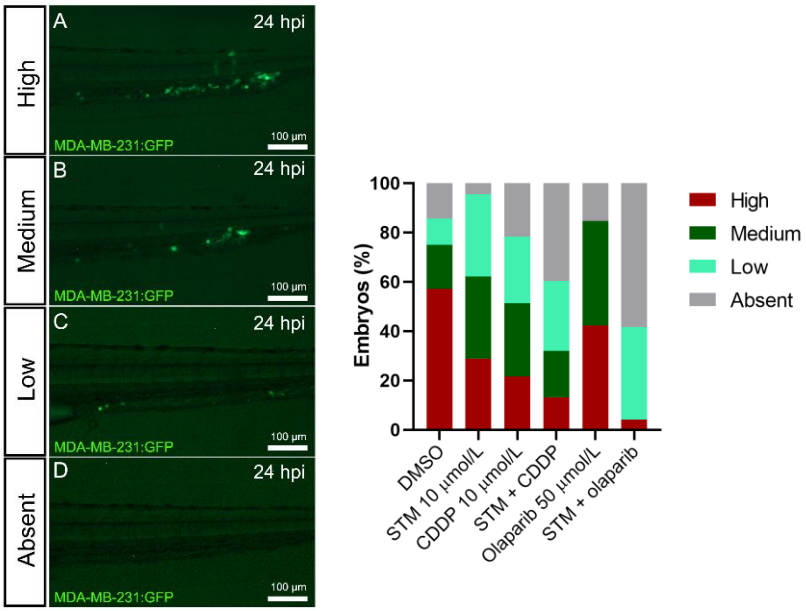

Figure 4.16. 48 hours post-fertilization (hpf) zebrafish embryos were directly engrafted into the perivitelline sac (PVS) with MDA-MB-231 GFP+ cells. Left panel, representative fluorescence stereomicroscope images of the CHT region (lateral view, anterior to the left), containing the extravasated GFP+ cells 24 hours post-injection (hpi), which displays the 4 discrete classes categorizing the xenotransplants (high, medium, low, absent). Right panel, evaluation of cells ability to extravasate through 48 hpf Zebrafish embryos xenograft. Each bar represents mean value % of larvae at 24 hpi calculated from, at least, two independent experiments. Total number of embryos analyzed was 213, divided as follows: DMSO (n = 28), STM2457 (n = 45), CDDP (n = 37), STM2457+CDDP (n = 53), olaparib (n = 26), STM2457+olaparib (n = 24).

4.10 STM2457 synergizes with genotoxic therapy in patient-derived organoids (BCOs)

Finally, we proceeded to assess the impact of STM2457 in patient-derived organoids (PDOs), which currently represent a pre-clinical model for TNBC studies. Given their ability to faithfully recapitulate the original tumor due to their derivation from tumor biopsies, PDOs provide a versatile and patient-specific platform for studying tumor biology, testing drugs, and advancing personalized medicine approaches. Hence, we tested the efficacy of STM2457 in two different patient-derived organoids (BCO-21, BCO-35) obtained from TNBC patients with wild-type BRCA1/2 genes (Figure 4.17).

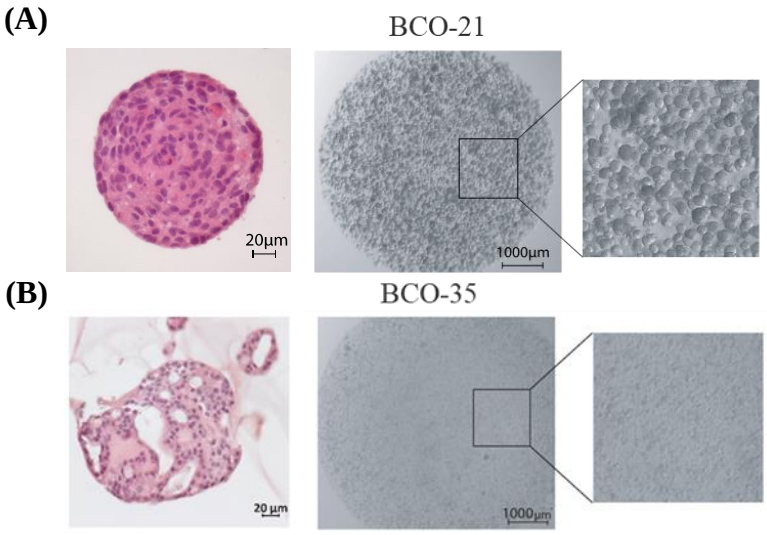

Figure 4.17. Representative images showing haematoxylin-eosin staining and bright-field images of (A) BCO-21 and (B) BCO-35.

First, we determined the IC_{50} with single treatment of STM2457, olaparib and carboplatin, a platinum-based chemotherapeutic drug that is utilized in TNBC standard chemotherapy (Figure 4.18). Indeed, at this point of the research, as we shifted to study STM2457 impact in an *in vivo* system that more closely mimics human physiology, we considered using carboplatin, since cisplatin is characterized by a greater number of side effects, particularly concerning renal and neurological aspects, in comparison to other DNA damaging agents, such as carboplatin.

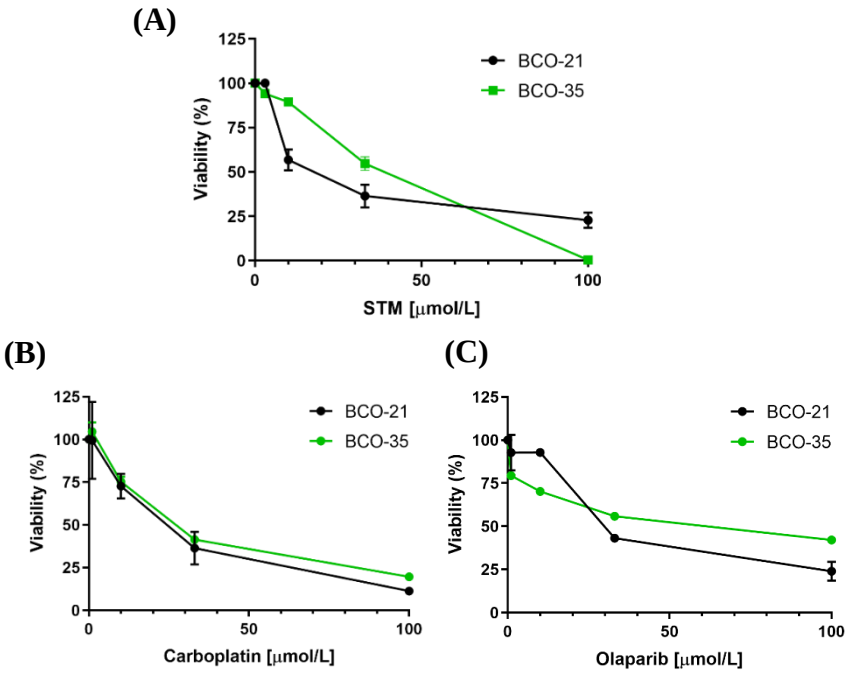

Figure 4.18. Cytotoxic effects of (A) STM2457, (B) carboplatin and (C) olaparib on patient-derived breast cancer organoids (BCO-21, BCO-35). Cells were exposed to various concentrations (µmol/L) of the drugs for 5 days and viability was evaluated by Cell Titer Glo 3D assay.

Consistent with findings in TNBC cell lines, we confirmed a robust decrease in cell viability following catalytic inhibition of METTL3. Subsequently, we investigated whether inhibiting METTL3 enhances the sensitivity of BCOs (BCO-21 and BCO-35) to DNA damaging therapy, as previously demonstrated in TNBC cell lines. We selected two STM2457 doses, suboptimal (5 µmol/L) and optimal (10 µmol/L), to test the effect of combined treatments. Notably, the combination treatment of STM2457, at both optimal and suboptimal doses, with carboplatin, synergized with DNA damaging agents in both BCO lines (Figure 4.19).

(A)

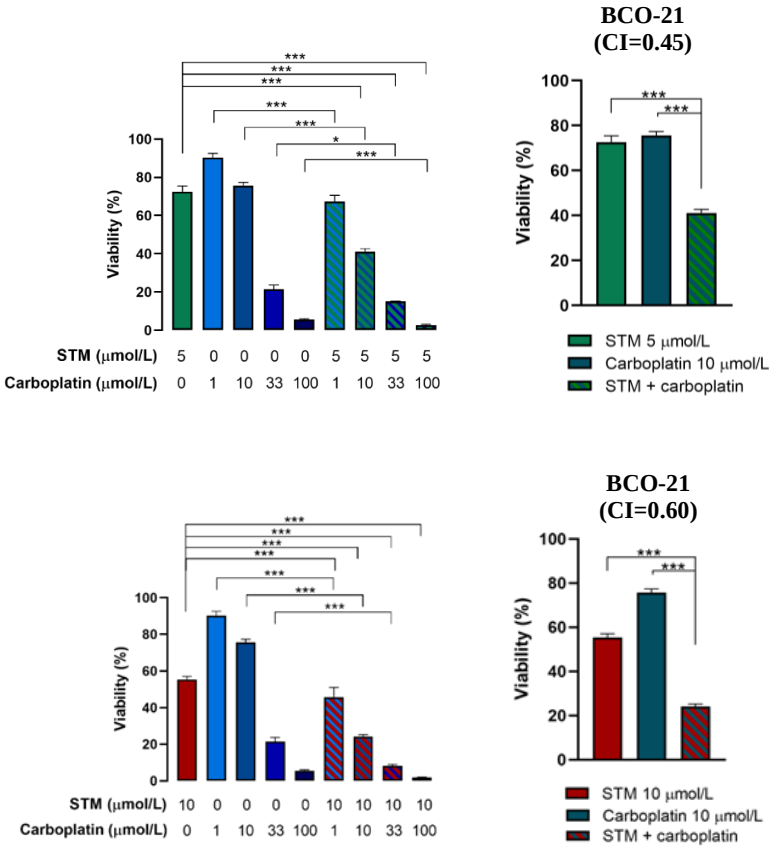

(B)

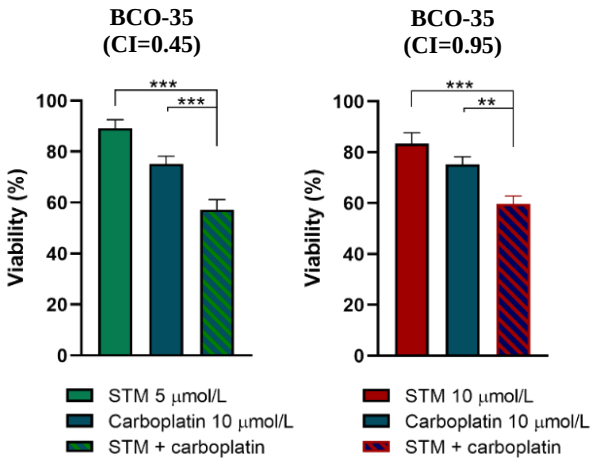

Figure 4.19. Synergistic effects of STM2457 and carboplatin on viability of the two different BCOs, (A) BCO-21 and (B) BCO-35. The two lines of BCOs were exposed for 5 days) to combined treatments with suboptimal (5 μmol/L) and optimal (10 μmol/L) doses of STM2457, carboplatin (10 μmol/L). Combination Index (CI)<1 indicates synergism. All results are expressed as the mean ± SEM derived from triplicates. Statistical analyses were performed on GraphPad software, by using one-way ANOVA Dunnett's multiple comparisons test where the significance of the combined treatment was calculated on its related single treatments * $p<0.05$, ** $p<0.01$, *** $p<0.001$, $p<0.0001$.

Finally, we tested combination treatment with STM2457 and olaparib on BCO-21 (Figure 4.20). Intriguingly, even though BCO-21 was genotyped as wild-type for BRCA1/2, it exhibited a strong sensitivity to STM2457 and to the combined treatment, in line with results in cell lines.

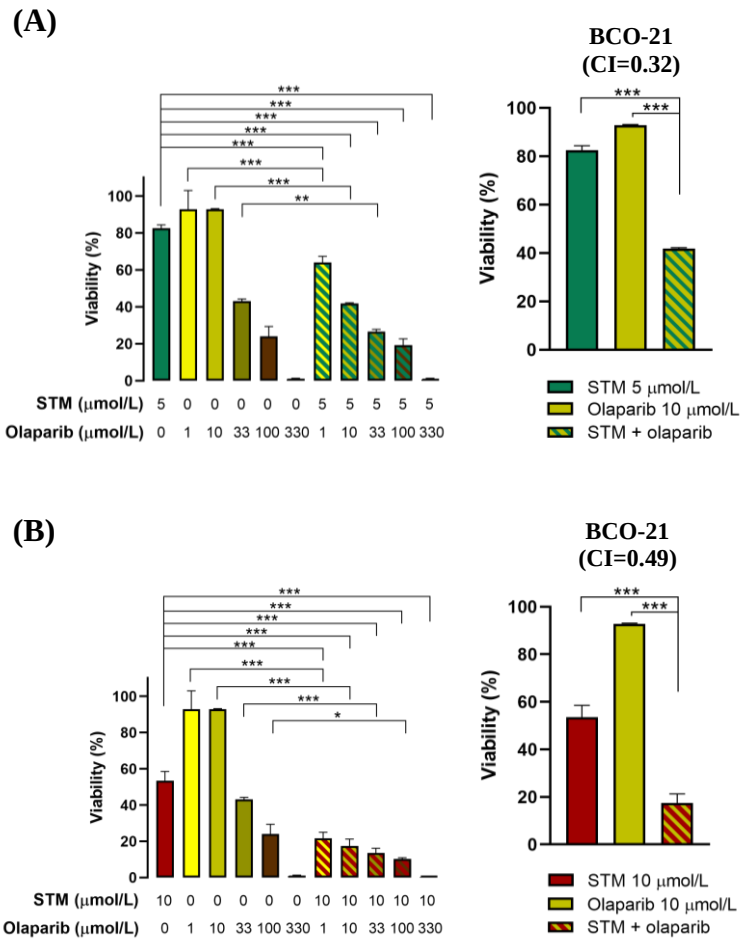

Figure 4.20. Synergistic effects of STM2457 and olaparib on viability of BCO-21. BCO-21 was exposed for 5 days to combined treatments with (A) suboptimal (5 μmol/L) and (B) optimal (10 μmol/L) doses of STM2457 and olaparib (10 μmol/L). Combination Index (CI)<1 indicates synergism. All results are expressed as the mean ± SEM derived from triplicates. Statistical analyses were performed on GraphPad software, by using one-way ANOVA Dunnett's multiple comparisons test where the significance of the combined treatment was calculated on its related single treatments * $p<0.05$, ** $p<0.01$, *** $p<0.001$, $p<0.0001$.

5. DISCUSSION

Breast cancer stands out as one of the major forms of malignancy affecting women. As highlighted in the cancer epidemiological research conducted by the American Cancer Society, breast cancer holds the unfortunate distinction of being the most prevalent cancer and the second most frequent cause of cancer-related fatalities among women in the United States in 2020[106]. On a global scale, female breast cancer continues to impose a significant health burden across the vast majority of territories, spanning both developing and developed nations. Despite the existence of various treatment approaches, the prognosis for breast cancer remains discouraging. Consequently, there is a growing imperative to identify additional targets that could enhance early diagnosis and facilitate more effective treatment.

Due to the pronounced diversity within breast cancer, notable distinctions exist in the diagnosis, treatment approaches, and prognoses across its various subtypes. Notably, based on the expression of the hormone receptors estrogen (ER) and progesterone (PR) and the human epidermal growth factor receptor 2 (HER2), four molecular subtypes of breast cancer have been classified, luminal A, luminal B, HER2 positive and basal-like or triple-negative (TNBC). Although both luminal A and B are ER and PR positive, the later one has a worst prognosis and is either HER positive or negative with high levels of the proliferation marker Ki-67. The HER2 subtype is ER and PR negative but positive for HER2. For this reason, the primary choice for treating luminal A and luminal B tumors typically involves endocrine therapy, towards which TNBC is not sensitive, presenting a triple negative immunophenotype (ER, PR and HER2 negative), increased proliferation rate and the highest incidence of relapse[107]. Thus, beyond offering prognostic insights, these molecular subtypes serve to assess clinical behaviours and responses to treatments. Nevertheless, the intrinsic diversity within breast

cancer poses challenges for comprehensive characterization solely based on the mentioned histopathologic parameters. The heterogeneity of breast cancer manifests internally through disparities in the genome, transcriptome, proteome, and metabolome.

Indeed, our comprehension of cancer origins has undergone a substantial transformation in recent years. Initially perceived as exclusively genetic, it is now recognized as a condition influenced by both genetic, epigenetic and epitranscriptomic factors. While conventional epigenetic alterations, such as disruptions in DNA methylation and histone modification, contribute to cancer, a ground-breaking revelation has emerged, showing that chemical modifications of RNA also play an important role in cancer. Notably, the discovery of RNA modifications opens a new era in investigating the evolution and progression of breast cancer.

Multiple studies shed light on the connection between N6-methyladenosine (m^6A) regulators and hallmarks of cancer. M^6A is an RNA modification, prevalently present on messenger RNAs, which regulates each step of RNA metabolism. Despite the majority of evidences in literature show METTL3 as a oncogene in most cancer types, including triple-negative breast cancer, it was also reported as tumor suppressor in some cases[108,109], suggesting how context-dependent and environmental factors may significantly infer study outcomes. This highlights the intricate and contradictory roles of METTL3, as well as other m^6A members, emphasizing the need for a more comprehensive understanding of the m^6A regulatory landscape. However, studies have demonstrated elevated m^6A methylation levels in breast cancer cells compared with those in healthy mammary epithelial cells, as also shown in this work. Yet, studies aiming to investigate on the role of m^6A regulators in breast cancer, including METTL3, were conducted through RNA interference or genome editing approaches. Although these methods can be efficient in studying molecular and cellular aspects *in vitro* and in animal models, they have limitations in the prospective of employing such strategies in

cancer therapies. In 2021, Yankova et al. designed and synthesized the first bioavailable selective inhibitor of the m^6A writer METTL3, named STM2457, furthermore showing the first demonstration of *in vivo* activity and therapeutic efficacy of an inhibitor of an RNA methyltransferase against cancer[99]. The advantages of using an inhibitor molecule instead of approaching a RNA interference strategy include characteristics such greater stability over time compared to RNA molecules, target specificity and *in vivo* efficacy. Indeed, inhibitory molecules may have a higher likelihood of reaching their targets within cells and tissues *in vivo*, as they are not subjected to the same cellular barriers that RNA can encounter, eventually making them more useful for the development of pharmacological therapies.

For the first time, we employed the use of STM2457 in different breast cancer models. To this aim, we assessed STM2457 efficacy on the most aggressive subtype of breast cancer, TNBC. Given the high heterogeneity within this subtype, STM2457 activity was tested on several TNBC cell lines, MDA-MB-231, MDA-MB-468, HCC1395, MDA-MB-436 and HCC1937, characterized by different morphological, histological, and genetic background. Notably, we highlighted the mutational status of the oncosuppressor BRCA1/2, which represents a prognostic marker in the management of TNBC treatment. BRCA1/2 wild-type cell lines and tumors usually manifest resistance towards chemotherapy agents. Therefore, we focused our study on MDA-MB-231 cell line, which carries homologous wild-type BRCA1/2 and therefore seemed to be the most promising candidate to prove STM2457 efficacy, since its aggressive and invasive properties. Furthermore, MDA-MB-231 cells present a high nuclear ratio of METTL3 protein, which was recently correlated with nodal metastasis in human cancers[103].

Parallelly, prior to proceed into the investigation of STM2457 as a valuable anti-tumoral drug, we tested MCF10A as the normal counterpart cell line. Testing an anti-tumoral drug on normal tissue is crucial for toxicity assessment and allows the identification of

possible adverse effects which may help in dose optimization. As previously anticipated in the pioneering work[99], where STM2457 did not show toxicity or long-term alterations in normal blood cell counts or body weight, we did not find a robust change in viability of the healthy cell line. Indeed, while MCF10A was not strongly affected by STM2457 activity, in TNBC we found a significant effect on the reduction of cell proliferation and viability, along with inability to form colonies and migrate *in vitro* and *in vivo* in zebrafish, thus confirming STM2457 anti-tumor properties.

Once the effect of STM2457 on the cell lines was ascertained, we verified the specificity of the inhibitory molecule using gene silencing, to establish that the recognized phenotype was due to the inhibition of METTL3 methyltransferase activity. The observed trend was, indeed, comparable to STM2457-induced METTL3 inhibition. However, small variations in treatment timing and intensity of the observed effects might be attributed to the different approaches used. Specifically, the inhibitor administered to the cell needs to enter the nucleus, where the majority of METTL3 is located, to exert inhibition of the catalytically active METTL3. In contrast, the genetic silencing of METTL3 required induction upon doxycycline treatment, which was used in our Tet-On gene expression system.

Another aspect to evaluate in the use of STM2457 was the assessment of the effective functionality of the molecule in inhibiting METTL3 methyltransferase activity. Indeed, we measured m^6A levels both globally and specifically on mRNAs that showed high levels of m^6A in MDA-MB-231 cells (MYC, BiP, WTAP mRNAs). In details, the reduction in m^6A abundance observed in both the MDA-MB-231 tumor cell line and the healthy MCF10A line demonstrates that the observed result was determined by the concrete reduction of m^6A levels.

To identify the molecular pathways affected by METTL3 catalytic inhibition, we performed RNA-sequencing analysis of MDA-MB-231 cells, treated with STM2457 10 μmol/L for 48 hours. Dose concentration and timing of the analysis were established to assess

the possible modulation of gene expression induced by STM2457 at a concentration below its IC_{50} in the mentioned cell line and for a sufficient period of time for a complete turnover of mRNAs to observe a significant change in mRNA profiles. Interestingly, gene ontology (GO) analysis showed a significant downregulation of biological processes involved in cell proliferation, translation, and DNA repair. This result is consistent with previous analyses performed upon METTL3 knockdown in breast cancer cells[88] and, most importantly, upon METTL3 inhibition by STM2457 in AML cell lines[99]. To assess whether the altered gene expression could be attributed to the inhibition of m^6A modification, we integrated RNA-seq analysis with the m^6A distribution across the transcriptome (MeRIP-seq) to detect genes that were both differentially expressed and m^6A-methylated. Among the overlapping genes, the most represented classes were cell cycle and DNA damage, meaning that genes belonging to these classes were both highly downregulated and highly methylated. We specifically focused on DNA damage, as it has been identified as a critical pathway regulated by METTL3 and is relevant to TNBC therapy.

Evidence in literature suggested the role of the m^6A writer METTL3 in DNA damage repair across various tumors, including breast cancer[89]. Indeed, we observed decreased BRCA1 protein levels and a concomitant increase of γ-H2AX protein levels, suggesting an inactivating role of m^6A modification in the DDR (DNA damage response), in accordance to downregulated class in RNA-seq. Despite the slight downregulation of BRCA1 expression levels in the RNA-seq analysis conducted on STM2457-treated cells, it is plausible that BRCA1 could undergo post-transcriptional regulation, potentially by YTHDF1[89] or other mechanisms. These mechanisms might involve both direct and indirect pathways through which m^6A modification could influence the DNA damage response.

Considering the multitude of advantages linked to combined chemotherapy[104], particularly in highly heterogeneous tumors like

TNBC, we explored the impact of METTL3 inhibition when combined with DNA-damaging agents. The use of combination chemotherapy is justified by several reasons. The combined use of different drugs can target multiple signaling pathways and molecular targets, increasing damage to tumor cells, and reducing the likelihood of developing drug resistance. Furthermore, some drugs might be more effective at targeting cells in a specific phase of the cell cycle, while others might have a more systemic effect. Combination therapy can allow for lower doses of each drug, usually sub-IC_{50} concentrations, thereby reducing the intensity of side effects associated with higher doses of a single drug. Ultimately, it represents a promising strategy to treat TNBC heterogeneity, referring to the presence of different cellular subpopulations within a tumor, thereby targeting a broader range of tumor cells. Therefore, we combined STM2457 with cisplatin and olaparib, which are direct and indirect inducers of DNA damage, respectively, by covalently bind to DNA and by inhibiting PARP protein. Cell count analysis and apoptosis evaluation upon combination treatment of STM2457 with cisplatin or olaparib showed that TNBC cells undergo proliferation arrest when treated with cisplatin or olaparib alone, while the combination of both STM2457+cisplatin and STM2457+olaparib strongly sensitized TNBC cells to DNA-damaging stimuli by triggering a significant apoptotic response. This result was partially explained by the strong increase of DNA damage assessed by increase of γH2AX levels in the combined treatments.

STM2457 impact on TNBC was also evaluated on *in vivo* zebrafish model, which is a suitable model for metastasis. Due to their small size and transparency, these organisms enable the tracking of transplanted cells. Notably, we found a significant activity of STM2457 in sensibilizing MDA-MB-231 cells to cisplatin and olaparib, thereby robustly decreasing number and size of micrometastases of the xenotransplanted cells.

Finally, we tested the efficacy of STM2457 in patient-derived organoids (BCO-21, BCO-35) derived from TNBC patients. To

date, the development of organoid technology opens new avenues for testing and development therapeutic approaches in a pre-clinical setting. Remarkably, even though both BCO-21 and BCO-35 were genotyped as wild-type for BRCA1/2, which would suggest a poor response to DNA-damaging agents, they exhibited a strong sensitivity to STM2457 and showed synergism to combined treatments with DNA damaging agents, consistent with the results observed in cell lines. In light of the recognition of the necessity to test this inhibitor in other organoid lines and further model systems for a broader understanding of its molecular effects, both independently and in combination with DNA damage-inducing agents, this research serves as evidence for the potential of STM2457 as an anti-tumoral drug targeting m^6A in TNBC.

In conclusion, we demonstrated that STM2457 has an anti-tumor effect in TNBC. Furthermore, since enhanced METTL3 activity has been detected in multiple cancer types, this work suggests that METTL3 inhibitors, such as STM2457, might constitute a novel therapeutic option to improve the efficacy of DNA-damaging agents, overcome inherent resistance, and reduce side effects in cancer therapies (Figure 5.1). Ultimately, this also provides a rationale for future investigations of combined pharmacological inhibition of METTL3.

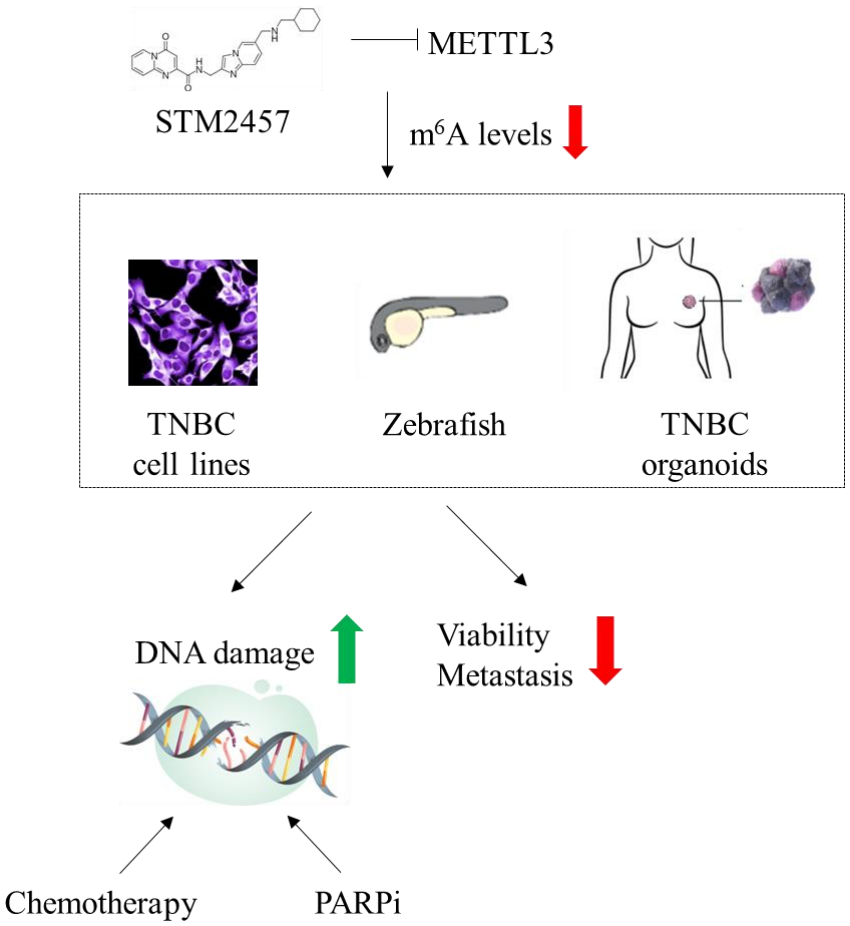

Figure 5.1. m^6A depletion following METTL3 inhibition by STM2457 sensitizes TNBC *in vitro* and *in vivo* models to DNA damaging chemotherapy, CDDP (cisplatin), or olaparib (PARPi) and impairs the DNA damage response, thereby triggering apoptosis in wild-type BRCA1/2 TNBC cells, reducing TNBC organoids viability and metastasis in zebrafish.

6. MATERIALS AND METHODS

6.1 Cell cultures and reagents

Human breast adenocarcinoma cell lines MDA-MB-231 (CRM-HTB-26), MDA-MB-436 (HTB-130) MDA-MB-468 (HTB-132) were purchased from the American Type Culture Collection (ATCC, Manassas, VA, USA) and were cultured in Dulbecco's Modified Eagle Medium (DMEM) medium (Gibco, Thermo Fisher Scientific, Waltham, MA, USA) with 10% fetal bovine serum (FBS, Gibco), 1× L-Glutamine (Gibco), 1× Penicillin-Streptomycin (Gibco). Human breast ductal carcinoma cell lines HCC1395 (CRL-2324, ATCC) and HCC1937, kindly provided by Prof. Giuseppe Giannini (Sapienza University of Rome, Rome, Italy), were cultured in Roswell Park Memorial Institute (RPMI) medium 1640 (Gibco) with 10% FBS, 1× L-Glutamine, 1× Penicillin-Streptomycin. Non-tumoral breast epithelial cell line MCF-10A (CRL-10317, ATCC) were cultured in DMEM/F12 (Gibco) supplemented with 5% Horse Serum (Gibco), 1× L-Glutamine, 1× Penicillin-Streptomycin, 20 ng/mL Epidermal growth factor (EGF, PHG0311, Thermo Fisher Scientific), 0.5 mg/mL Hydrocortisone (A16292, Thermo Fisher Scientific), 10 µg/mL Insulin (A11382I; Gibco). All cell lines were growth at 37°C under an atmosphere containing 5% CO2. Cell lines were routinely tested for mycoplasma contamination with LookOut Mycoplasma PCR Detection Kit (Merck KGaA, Darmstadt, Germany). STM2457 and olaparib were synthetized as previously described[100,110]. Green fluorescent protein (GFP) expressing MDA-MB-231 cell lines were obtained by stable integration with piggyBac transposon vector ePB-PGK-GFP-BSD[111], as described[95].

6.2 Patient-derived breast cancer organoids

Breast cancer organoids (BCO-21, BCO-35) were obtained from tumor biopsies and grown as described[112]. Briefly, breast cancer

tissue was placed in 60 mm Petri dishes with advanced DMEM/F12 containing 1× Glutamax (35050038, Thermo Fisher Scientific), 10 mmol/L 4-(2-hydroxyethyl)-1-piperazineethanesulfonic acid (HEPES, Gibco), and antibiotics culture medium (AdDF + + +). Part of the tissue was fixed in formalin for histopathological and immunohistochemistry analysis, part was stored at − 80°C for DNA/RNA isolation. The remaining part was minced by surgical blades into small fragments for organoids generation and digested in 10 mL AdDF + + + supplemented with 5 µmol/L Rhodopsin (RHO)/ Rho Associated Coiled-Coil Containing Protein Kinase (ROCK) pathway inhibitor (Y-27632, Tocris Bioscience, Minneapolis, MN, USA) containing 4 mg/ml Collagenase II (Thermo Fisher Scientific) on an orbital shaker at 37°C for 30 min - 60 min. The cell suspension was filtered with a magnetic-activated cell sorting (MACS) SmartStrainer 100 µm (130-098-463, Miltenyi Biotec, Bergisch Gladbach, Germany), placed on a 50 mL tube and washed with 10 mL of phosphate buffered saline (PBS) and centrifugated at 490 g for 5 min at 4°C. The pellet was incubated with 1 mL red blood cell lysis buffer for 5 min at room temperature and washed with 10 mL of PBS and pelleted. Cells pellet was embedded in undiluted (100%) Cultrex growth factor reduced basement membrane extract (BME) type 2 (Trevigen; Thermo Fisher Scientific) on ice and 40 µL drops of BME cell suspension were allowed to solidify to a pre-warmed 24 well suspension culture plates (Euroclone, Pero, MI, Italy). The plate was placed at 37°C for 30 min to allow the Matrigel to polymerize and then were added 500 µL of growing medium and incubated at 37°C in humidified air containing 5% CO2. Organoid culture medium was AdDF + + + supplemented with the component listed below. Medium was changed every 3–4 days and organoids were passaged every 2 weeks by enzymatic digestion with Triple Express (Gibco) for 10 min at 37°C. After rinsing in PBS, organoid fragments were resuspended in cold BME and reseeded as 1:4 ratio. BCO medium components: R-spondin1 10% conditioned medium (Sigma-

Aldrich), Noggin 10% conditioned medium (Sigma-Aldrich), 1× B27 + VitA, Nicotinamide (10 mmol/L, Sigma-Aldrich), N-acetylcysteine (1.25 mmol/L, Sigma-Aldrich), Primocin (100 µg/mL, Thermo Fisher), Hydrocortisone (0.5 µg/mL, Sigma-Aldrich), β-estradiol (100 nmol/L, Sigma-Aldrich), Forskolin (10 µmol/L, Sigma-Aldrich), Y-27632 (5 µmol/L, Sigma-Aldrich), Heregulin B1 (5 nmol/L, Sigma-Aldrich), FGF-7 (5 ng/mL, Sigma-Aldrich), FGF-10 (20 ng/mL, Sigma-Aldrich), A83-01 (0.5 µmol/L, Sigma-Aldrich), EGF (5 ng/mL, Sigma-Aldrich), SB202190 (1 µmol/L, Sigma-Aldrich).

6.3 Cell growth and viability analysis

Data for growth curves were obtained with the Countess 3 Automated Cell Counter (Thermo Fisher Scientific) and trypan blue staining. Cell viability was measured by MTT [3-(4,5-dimethylthiazol-2-yl)-2,5 diphenyl tetrazolium bromide] assay using the CellTiter 96® Non-Radioactive Cell Proliferation Assay (Promega Italia, Milan, Italy). Cell apoptosis was analyzed by flow cytometry using propidium iodide (Merck KGaA, Darmstadt, Germany) exclusion assay. BCO viability was performed as previously described110. Drug dose–response curves were visualized using linear regression analysis (setting: log(inhibitor) versus normalized response). Half-maximal inhibitory concentration (IC_{50}) values were determined from fitting curves. For synergic interaction analyses in BCO, organoids were treated with each drug at different concentrations, both alone and in conjunction with suboptimal doses of the other substance. The effects of the drug combinations were evaluated using combination index (CI) values computed with the Compusyn software (Biosoft, Ferguson, MO, USA). CI < 1 indicates synergism.

6.4 Colony formation assay

Cell lines were plated into 6-well plates at 2×103 cells/well and treated with dimethyl sulfoxide (DMSO, Sigma-Aldrich, St. Louis, MO, USA) and STM2457 every 72 hours. Colonies were fixed in

methanol and stained with 0.5% crystal violet (C8470, Amresco, San Diego, CA, USA) and 20% methanol (Sigma-Aldrich) for at least 30 min. Colonies were photographed and counted by ImageJ software (version 1.8.0, National Institutes of Health, Bethesda, MD, USA).

6.5 Wound healing assay

MDA-MB-231 cells were plated into 12-well plates at 4×105 cells/well. Scratch was performed in the middle of the cell monolayer prior to treatment with DMSO and STM2457 in FBS-free DMEM medium, to avoid cell proliferation bias. Wound closure was followed up to 24 hours and wound areas were measured with ImageJ software. Quantification of wound-healing assay was calculated as percentage of wound closure: [(At0 – At1)/At0 × 100] where At0 is the initial wound area and At1 is the wound area 24 hours after the initial scratch.

6.6 Quantification of global N6-methyladenosine (m^6A) levels

Global quantification of m6A levels was performed using the EpiQuik m6A RNA methylation quantification Kit (EpigenTek, Farmingdale, NY, USA) from purified mRNA, according to manufacturer instructions. In brief, mRNA was isolated from total RNA after 48 hours of STM2457 10μmol/L using two rounds of purification with the Dynabeads mRNA purification kit (Thermo Fisher), then 50 ng of purified mRNA were utilized form m6A quantification.

6.7 m^6A Immunoprecipitation-qPCR

Total RNA was extracted using Directzol RNA Miniprep kit (Zymo research) and m6A immunoprecipitation was performed by using the Magna MeRIP™ m6A Kit (Merck), according to the manufacturer's instruction. Reverse transcription to cDNA was performed with the SuperScript VILO cDNA Synthesis Kit (Thermo Fisher Scientific) and qPCR was performed using a

SYBR™ Green PCR Master Mix (Thermo Fisher Scientific), according to the manufacturer's instructions.

Primers used in qPCR:
c-MYC _FW: AGCTGCTTAGACGCTGGATT
c-MYC_REV: AAGTTCTCCTCCTCGTCGC
BiP_FW: AGGAGGACAAGAAGGAGGAC
BiP_RV: GAGTGAAGGCGACATAGGAC
HPRT_FW: GCCATCACATTGTAGCCCTCTG
HPRT_REV: TTTATGTCCCCTGTTGACTGGTC
WTAP_ FW: CCCCAAGTACCAGCAGGACT
WTAP_ REV: TCCGTTTGTCAGACGACTGC

6.8 RNA sequencing and Methylated RNA Immunoprecipitation Sequencing (MeRIP) sequencing

Total RNA was extracted using Directzol RNA Miniprep kit (Zymo research, Irvine, CA, USA) according to manufacturer instructions. Total RNA from triplicates was sent to Procomcure Next Generation Sequencing (NGS; Vienna, AU) for library preparation using the Nextflex Rapid Directional RNA-Seq kit 2.0 Kit with Poly(A) Beads 2.0 (PerkinElmer, Walltam, MA, USA) and subjected to sequencing (2 × 150 bp paired-end) on an Illumina Novaseq 6000 system (Illumina, San Diego, CA, USA). The RNA-seq data were analyzed with the Artificial Intelligence RNA-seq Software as a Service (SaaS) platform (https://transcriptomics.cloud). DESeq2 software was then used for the identification of differentially expressed genes. Genes were considered differentially expressed if the adjusted P value of the logarithm of the fold-change was less than or equal to 0.05. MeRIP sequencing dataset in MDA-MB231 was obtained from Gene Expression Omnibus (GEO) GSE183014 (https://www.ncbi.nlm.nih.gov/geo/query/acc.cgi?acc=GSE183014). Integrative Genomics Viewer (IGV) [10] was used to visualize the distribution and abundance of m6A peaks on each mRNA

transcript. Enrichment analysis (P-value cutoff 0.05) based on the Gene Ontology (GO) of biological processes was used to identify the most represented gene functions.
Hypergeometric analysis was used to calculate the significance of the overlap between differentially expressed and m6A methylated genes using the formula:

$P(A|B) = (N * K) / [M * (M - 1)]$
where:
P(A|B) is the probability that a dysregulated gene is also m6A methylated
N is the total number of expressed genes
K is the number of genes that are dysregulated
M is the number of genes that are m6A methylated

6.9 Immunoblot analysis
Immunoblot analysis were performed as previously described [8]. Immunoblots were incubated with antibodies anti-METTL3 (1:1,000, EPR18810, Abcam, Cambridge, MA, USA), anti Phospho-Histone H2A.X-Ser139 (1:500, 20E3, Cell Signaling Technology, MA, USA), anti-glyceraldehyde-3-phosphate dehydrogenase (GAPDH)- horseradish peroxidase (HRP) conjugated (1:500, bsm-33033M-HRP, Bioss, Woburn, MA, USA), anti-vinculin (1:10,000, sc-73264, Santa Cruz Biotechnology, Texas, USA). Detection was carried out with Clarity Western ECL Blotting Substrate (BioRad, Hercules, CA, USA) using ChemiDocTM MP System and images were analysed using Image LabTM Software (BioRad,).

6.10 Immunofluorescence analysis
Immunofluorescence was performed as previously described [8]. Cells were washed with PBS and fixed with 4% formaldehyde solution (Sigma-Aldrich) for 10 minutes at room temperature. After permeabilization with 0.1% Triton X-100 (Sigma-Aldrich) for 10 min, cells were blocked with 3% Bovine Serum Albumin

(BSA) for 1 hour and incubated with the primary antibody anti-RAD51 (1:1,000, #ab176458, Abcam) overnight at 4°C. After two washes with Perm/Wash buffer (#554723, Becton Dickinson), cells were incubated with the secondary antibody Alexa Fluor 488-labeled goat anti-rabbit (#A-11034, Thermo Scientific) for 1h at room temperature. The nuclei were stained with Hoechst 33342 (Life Technologies) for 5 min in Perm/Wash buffer. Cells were then mounted in VECTASHIELD antifade mounting media (#H-1000, Vector Laboratories, Newark, CA, USA). Images were acquired using a LSM 900 confocal laser scanning microscope (Zeiss, Munich, Germany). RAD51 foci were counted by ImageJ software.

6.11 METTL3 knockdown

Inducible lentiviral constructs for METTL3 knockdown experiments were derived from Mission Lentiviral shRNA clones shMETTL3#1 (TRCN0000289812, Sigma-Aldrich, St. Louis, MO, USA), shMETTL3#2 (TRCN0000289814, Sigma-Aldrich) and SHC202 TRC2 (Non-Target shRNA Control, shSCR, Sigma-Aldrich). Lentiviral particles preparation, transduction and selection were performed as previously described95.

6.12 Larval zebrafish xenografts

48 hours post-fertilization (hpf) anesthetized zebrafish larvae were microinjected with GFP-positive MDA-MB-231 cells. Cells were resuspended in complete medium at a final concentration of 150 cells/nL, and 4 nL were inoculated into the perivitelline space. Injected larvae were immediately inspected under a fluorescent microscope for the presence of GFP-positive cells; non-injected zebrafish larvae were discarded, whereas successful ones were arrayed in 6 groups, one for each treatment [STM2457, olaparib, cisplatin (CDDP), STM2456+olaparib, STM2457+CDDP] and vehicle (DMSO) as control. The drugs were added to the E3 fish water at the following concentrations: 10 μmol/L (STM2457), 10 μmol/L (CDDP), 50 μmol/L (olaparib), and the xenografts were

incubated at 34°C. At 24-hours post-injection (hpi), the larvae were anesthetized, individually placed on a microscope slide, and classified based on the extent of the area covered by the extravasated cells using an inverted fluorescent microscope. Since the GFP-positive extravasated cancer cells could be seen predominantly around the caudal hematopoietic tissue (CHT) region, we chose this area to categorize the larvae in 4 discrete classes: high, medium, low, absent. At least two independent biological replicates were performed. The number (n) of larvae for each experiment is indicated in the figure legend.

6.13 Statistical analysis

Cell growth and viability analysis were analyzed by two-way analysis of variance (ANOVA) using Dunnett's multiple comparison test, wound healing assay data were analyzed using two-tailed unpaired Student's t-test, Western blot and Immunofluorescence analysis were conducted by Student's t-test and one-way ANOVA using Tukey's multiple comparison test. All statistical tests were performed using the GraphPad Prism 8 software (GraphPad Software, San Diego, CA, USA). Analyses were performed from at least three independent replicates ($n \geq 3$). All data are reported as mean ± standard deviation (SD). A P value <0.05 was considered statistically significant.

7. REFERENCES

1. Desrosiers, R., Friderici, K. & Rottman, F. Identification of methylated nucleosides in messenger RNA from Novikoff hepatoma cells. *Proc Natl Acad Sci U S A* **71**, 3971–3975 (1974).
2. Perry, R. P., Kelley, D. E., Friderici, K. & Rottman, F. The methylated constituents of L cell messenger RNA: Evidence for an unusual cluster at the 5′ terminus. *Cell* **4**, 387–394 (1975).
3. Adams, J. M. & Cory, S. Modified nucleosides and bizarre 5′-termini in mouse myeloma mRNA. *Nature* **255**, 28–33 (1975).
4. Dominissini, D. *et al.* Topology of the human and mouse m6A RNA methylomes revealed by m6A-seq. *Nature* **485**, 201–206 (2012).
5. Meyer, K. D. *et al.* Comprehensive Analysis of mRNA Methylation Reveals Enrichment in 3′ UTRs and near Stop Codons. *Cell* **149**, 1635–1646 (2012).
6. Wei, C. M., Gershowitz, A. & Moss, B. 5'-Terminal and internal methylated nucleotide sequences in HeLa cell mRNA. *Biochemistry* **15**, 397–401 (1976).
7. Zhao, B. S. *et al.* m6A-dependent maternal mRNA clearance facilitates zebrafish maternal-to-zygotic transition. *Nature* **542**, 475–478 (2017).
8. Levis, R. & Penman, S. 5′-Terminal structures of poly(A)+ cytoplasmic messenger RNA and of poly(A)+ and poly(A)− heterogeneous nuclear RNA of cells of the dipteran Drosophila melanogaster. *Journal of Molecular Biology* **120**, 487–515 (1978).
9. Nichols, J. L. N6-methyladenosine in maize poly(A)-containing RNA. *Plant Science Letters* **15**, 357–361 (1979).
10. Kennedy, T. D. & Lane, B. G. Wheat embryo ribonucleates. XIII. Methyl-substituted nucleoside constituents and 5′-terminal dinucleotide sequences in bulk poly(A)-rich RNA from imbibing wheat embryos. *Can. J. Biochem.* **57**, 927–931 (1979).

11. Zhong, S. *et al.* MTA Is an *Arabidopsis* Messenger RNA Adenosine Methylase and Interacts with a Homolog of a Sex-Specific Splicing Factor. *The Plant Cell* **20**, 1278–1288 (2008).
12. Clancy, M. J., Shambaugh, M. E., Timpte, C. S. & Bokar, J. A. Induction of sporulation in Saccharomyces cerevisiae leads to the formation of N6-methyladenosine in mRNA: a potential mechanism for the activity of the IME4 gene. *Nucleic Acids Res* **30**, 4509–4518 (2002).
13. Beemon, K. & Keith, J. Localization of N6-methyladenosine in the Rous sarcoma virus genome. *Journal of Molecular Biology* **113**, 165–179 (1977).
14. Aloni, Y., Dhar, R. & Khoury, G. Methylation of nuclear simian virus 40 RNAs. *J Virol* **32**, 52–60 (1979).
15. Huang, H. *et al.* Histone H3 trimethylation at lysine 36 guides m6A RNA modification co-transcriptionally. *Nature* **567**, 414–419 (2019).
16. Bokar, J. A., Shambaugh, M. E., Polayes, D., Matera, A. G. & Rottman, F. M. Purification and cDNA cloning of the AdoMet-binding subunit of the human mRNA (N6-adenosine)-methyltransferase. *RNA* **3**, 1233–1247 (1997).
17. Liu, J. *et al.* A METTL3–METTL14 complex mediates mammalian nuclear RNA N6-adenosine methylation. *Nat Chem Biol* **10**, 93–95 (2014).
18. Ping, X.-L. *et al.* Mammalian WTAP is a regulatory subunit of the RNA N6-methyladenosine methyltransferase. *Cell Res* **24**, 177–189 (2014).
19. Huang, W. *et al.* N6-methyladenosine methyltransferases: functions, regulation, and clinical potential. *Journal of Hematology & Oncology* **14**, 117 (2021).
20. Deng, X., Qing, Y., Horne, D., Huang, H. & Chen, J. The roles and implications of RNA m6A modification in cancer. *Nat Rev Clin Oncol* **20**, 507–526 (2023).
21. Fu, Y., Dominissini, D., Rechavi, G. & He, C. Gene expression regulation mediated through reversible m6A RNA methylation. *Nat Rev Genet* **15**, 293–306 (2014).

22. Jia, G. *et al.* N6-Methyladenosine in Nuclear RNA is a Major Substrate of the Obesity-Associated FTO. *Nat Chem Biol* **7**, 885–887 (2011).
23. Zheng, G. *et al.* ALKBH5 Is a Mammalian RNA Demethylase that Impacts RNA Metabolism and Mouse Fertility. *Mol Cell* **49**, 18–29 (2013).
24. Mauer, J. *et al.* FTO controls reversible m6Am RNA methylation during snRNA biogenesis. *Nat Chem Biol* **15**, 340–347 (2019).
25. Xiao, W. *et al.* Nuclear m6A Reader YTHDC1 Regulates mRNA Splicing. *Molecular Cell* **61**, 507–519 (2016).
26. Wang, X. *et al.* m6A-dependent regulation of messenger RNA stability. *Nature* **505**, 117–120 (2014).
27. Wang, X. *et al.* N6-methyladenosine Modulates Messenger RNA Translation Efficiency. *Cell* **161**, 1388–1399 (2015).
28. Xu, C. *et al.* Structural basis for selective binding of m6A RNA by the YTHDC1 YTH domain. *Nat Chem Biol* **10**, 927–929 (2014).
29. Du, H. *et al.* YTHDF2 destabilizes m6A-containing RNA through direct recruitment of the CCR4–NOT deadenylase complex. *Nat Commun* **7**, 12626 (2016).
30. Shi, H. *et al.* YTHDF3 facilitates translation and decay of N6-methyladenosine-modified RNA. *Cell Res* **27**, 315–328 (2017).
31. Zaccara, S. & Jaffrey, S. R. A Unified Model for the Function of YTHDF Proteins in Regulating m6A-Modified mRNA. *Cell* **181**, 1582-1595.e18 (2020).
32. Hsu, P. J. *et al.* Ythdc2 is an N6-methyladenosine binding protein that regulates mammalian spermatogenesis. *Cell Res* **27**, 1115–1127 (2017).
33. Huang, H. *et al.* Recognition of RNA N6-methyladenosine by IGF2BP Proteins Enhances mRNA Stability and Translation. *Nat Cell Biol* **20**, 285–295 (2018).
34. Liu, N. *et al.* N6-methyladenosine-dependent RNA structural switches regulate RNA-protein interactions. *Nature* **518**, 560–564 (2015).

35. Edupuganti, R. R. *et al.* N6-methyladenosine (m6A) recruits and repels proteins to regulate mRNA homeostasis. *Nat Struct Mol Biol* **24**, 870–878 (2017).
36. Geula, S. *et al.* m ^{6} A mRNA methylation facilitates resolution of naïve pluripotency toward differentiation. *Science* **347**, 1002–1006 (2015).
37. Sui, X. *et al.* METTL3-mediated m ^{6} A is required for murine oocyte maturation and maternal-to-zygotic transition. *Cell Cycle* **19**, 391–404 (2020).
38. Xia, H. *et al. Mettl3* Mutation Disrupts Gamete Maturation and Reduces Fertility in Zebrafish. *Genetics* **208**, 729–743 (2018).
39. Lence, T. *et al.* m6A modulates neuronal functions and sex determination in Drosophila. *Nature* **540**, 242–247 (2016).
40. Patil, D. P. *et al.* m6A RNA methylation promotes XIST-mediated transcriptional repression. *Nature* **537**, 369–373 (2016).
41. Wu, Y. *et al.* Mettl3-mediated m6A RNA methylation regulates the fate of bone marrow mesenchymal stem cells and osteoporosis. *Nat Commun* **9**, 4772 (2018).
42. Fischer, J. *et al.* Inactivation of the Fto gene protects from obesity. *Nature* **458**, 894–898 (2009).
43. Koranda, J. L. *et al.* Mettl14 Is Essential for Epitranscriptomic Regulation of Striatal Function and Learning. *Neuron* **99**, 283-292.e5 (2018).
44. Engel, M. *et al.* The Role of m6A/m-RNA Methylation in Stress Response Regulation. *Neuron* **99**, 389-403.e9 (2018).
45. Lv, J. *et al.* Endothelial-specific m6A modulates mouse hematopoietic stem and progenitor cell development via Notch signaling. *Cell Res* **28**, 249–252 (2018).
46. Wang, H. *et al.* Loss of YTHDF2-mediated m6A-dependent mRNA clearance facilitates hematopoietic stem cell regeneration. *Cell Res* **28**, 1035–1038 (2018).
47. Yao, Q. J. *et al.* Mettl3–Mettl14 methyltransferase complex regulates the quiescence of adult hematopoietic stem cells. *Cell Res* **28**, 952–954 (2018).

48. Sung, H. *et al.* Global Cancer Statistics 2020: GLOBOCAN Estimates of Incidence and Mortality Worldwide for 36 Cancers in 185 Countries. *CA A Cancer J Clinicians* **71**, 209–249 (2021).
49. Danaei, G., Hoorn, S. V., Lopez, A. D., Murray, C. J. & Ezzati, M. Causes of cancer in the world: comparative risk assessment of nine behavioural and environmental risk factors. *The Lancet* **366**, 1784–1793 (2005).
50. Tan, P. H. *et al.* The 2019 World Health Organization classification of tumours of the breast. *Histopathology* **77**, 181–185 (2020).
51. Nolan, E., Lindeman, G. J. & Visvader, J. E. Deciphering breast cancer: from biology to the clinic. *Cell* **186**, 1708–1728 (2023).
52. Sørlie, T. *et al.* Gene expression patterns of breast carcinomas distinguish tumor subclasses with clinical implications. *Proc. Natl. Acad. Sci. U.S.A.* **98**, 10869–10874 (2001).
53. Perou, C. M. *et al.* Molecular portraits of human breast tumours. *Nature* **406**, 747–752 (2000).
54. Zagami, P. & Carey, L. A. Triple negative breast cancer: Pitfalls and progress. *npj Breast Cancer* **8**, 95 (2022).
55. Lehmann, B. D. *et al.* Identification of human triple-negative breast cancer subtypes and preclinical models for selection of targeted therapies. *J. Clin. Invest.* **121**, 2750–2767 (2011).
56. Thennavan, A. *et al.* Molecular analysis of TCGA breast cancer histologic types. *Cell Genomics* **1**, 100067 (2021).
57. Chung, W. *et al.* Single-cell RNA-seq enables comprehensive tumour and immune cell profiling in primary breast cancer. *Nat Commun* **8**, 15081 (2017).
58. Wagner, J. *et al.* A Single-Cell Atlas of the Tumor and Immune Ecosystem of Human Breast Cancer. *Cell* **177**, 1330-1345.e18 (2019).

59. Bianchini, G., De Angelis, C., Licata, L. & Gianni, L. Treatment landscape of triple-negative breast cancer — expanded options, evolving needs. *Nat Rev Clin Oncol* **19**, 91–113 (2022).
60. Hoxhaj, G. & Manning, B. D. The PI3K–AKT network at the interface of oncogenic signalling and cancer metabolism. *Nat Rev Cancer* **20**, 74–88 (2020).
61. Normanno, N. *et al.* Breast cancer cells with acquired resistance to the EGFR tyrosine kinase inhibitor gefitinib show persistent activation of MAPK signaling. *Breast Cancer Res Treat* **112**, 25–33 (2008).
62. Jacobson, A. Pembrolizumab Improves Outcomes in Early-Stage and Locally Advanced or Metastatic Triple-Negative Breast Cancer. *The Oncologist* **27**, S17–S18 (2022).
63. Kuchenbaecker, K. B. *et al.* Risks of Breast, Ovarian, and Contralateral Breast Cancer for *BRCA1* and *BRCA2* Mutation Carriers. *JAMA* **317**, 2402 (2017).
64. Robson, M. *et al.* Olaparib for Metastatic Breast Cancer in Patients with a Germline *BRCA* Mutation. *N Engl J Med* **377**, 523–533 (2017).
65. Loibl, S., Poortmans, P., Morrow, M., Denkert, C. & Curigliano, G. Breast cancer. *The Lancet* **397**, 1750–1769 (2021).
66. Cardillo, T. M. *et al.* Synthetic Lethality Exploitation by an Anti–Trop-2-SN-38 Antibody–Drug Conjugate, IMMU-132, Plus PARP Inhibitors in *BRCA1/2* –wild-type Triple-Negative Breast Cancer. *Clinical Cancer Research* **23**, 3405–3415 (2017).
67. Savas, P. *et al.* Clinical relevance of host immunity in breast cancer: from TILs to the clinic. *Nat Rev Clin Oncol* **13**, 228–241 (2016).
68. Xie, J. *et al.* The m6A methyltransferase METTL3 promotes the stemness and malignant progression of breast cancer by mediating m6A modification on SOX2. *J BUON* **26**, 444–449 (2021).
69. Cai, X. *et al.* HBXIP-elevated methyltransferase METTL3 promotes the progression of breast cancer via inhibiting tumor suppressor let-7g. *Cancer Letters* **415**, 11–19 (2018).

70. Wang, H., Xu, B. & Shi, J. N6-methyladenosine METTL3 promotes the breast cancer progression via targeting Bcl-2. *Gene* **722**, 144076 (2020).
71. Chen, F. *et al. N6* -Methyladenosine Regulates mRNA Stability and Translation Efficiency of KRT7 to Promote Breast Cancer Lung Metastasis. *Cancer Research* **81**, 2847–2860 (2021).
72. Zhao, C., Ling, X., Xia, Y., Yan, B. & Guan, Q. The m6A methyltransferase METTL3 controls epithelial-mesenchymal transition, migration and invasion of breast cancer through the MALAT1/miR-26b/HMGA2 axis. *Cancer Cell Int* **21**, 441 (2021).
73. Niu, Y. *et al.* RNA N6-methyladenosine demethylase FTO promotes breast tumor progression through inhibiting BNIP3. *Mol Cancer* **18**, 46 (2019).
74. Zhang, C. *et al.* Hypoxia induces the breast cancer stem cell phenotype by HIF-dependent and ALKBH5-mediated m ^{6} A-demethylation of NANOG mRNA. *Proc. Natl. Acad. Sci. U.S.A.* **113**, (2016).
75. Zhang, C. *et al.* Hypoxia-inducible factors regulate pluripotency factor expression by ZNF217- and ALKBH5-mediated modulation of RNA methylation in breast cancer cells. *Oncotarget* **7**, 64527–64542 (2016).
76. Anita, R., Paramasivam, A., Priyadharsini, J. V. & Chitra, S. The m6A readers YTHDF1 and YTHDF3 aberrations associated with metastasis and predict poor prognosis in breast cancer patients. *Am J Cancer Res* **10**, 2546–2554 (2020).
77. Chang, G. *et al.* YTHDF3 Induces the Translation of m6A-Enriched Gene Transcripts to Promote Breast Cancer Brain Metastasis. *Cancer Cell* **38**, 857-871.e7 (2020).
78. Hao, W. *et al.* Autophagy induction promoted by m6A reader YTHDF3 through translation upregulation of FOXO3 mRNA. *Nat Commun* **13**, 5845 (2022).
79. Einstein, J. M. *et al.* Inhibition of YTHDF2 triggers proteotoxic cell death in MYC-driven breast cancer. *Molecular Cell* **81**, 3048-3064.e9 (2021).

80. Gu, Y. *et al.* The evolving landscape of N6-methyladenosine modification in the tumor microenvironment. *Molecular Therapy* **29**, 1703–1715 (2021).
81. Dong, L. *et al.* The loss of RNA N6-adenosine methyltransferase Mettl14 in tumor-associated macrophages promotes CD8+ T cell dysfunction and tumor growth. *Cancer Cell* **39**, 945-957.e10 (2021).
82. Song, H. *et al.* METTL3-mediated m6A RNA methylation promotes the anti-tumour immunity of natural killer cells. *Nat Commun* **12**, 5522 (2021).
83. Lord, C. J. & Ashworth, A. The DNA damage response and cancer therapy. *Nature* **481**, 287–294 (2012).
84. Marechal, A. & Zou, L. DNA Damage Sensing by the ATM and ATR Kinases. *Cold Spring Harbor Perspectives in Biology* **5**, a012716–a012716 (2013).
85. Xiang, Y. *et al.* RNA m6A methylation regulates the ultraviolet-induced DNA damage response. *Nature* **543**, 573–576 (2017).
86. Abakir, A. *et al.* N6-methyladenosine regulates the stability of RNA:DNA hybrids in human cells. *Nat Genet* **52**, 48–55 (2020).
87. Zhang, C. *et al.* METTL3 and N6-Methyladenosine Promote Homologous Recombination-Mediated Repair of DSBs by Modulating DNA-RNA Hybrid Accumulation. *Molecular Cell* **79**, 425-442.e7 (2020).
88. Zhang, Q. *et al.* The RNA demethylase FTO is required for maintenance of bone mass and functions to protect osteoblasts from genotoxic damage. *Proc. Natl. Acad. Sci. U.S.A.* **116**, 17980–17989 (2019).
89. Li, E. *et al.* METTL3 promotes homologous recombination repair and modulates chemotherapeutic response in breast cancer by regulating the EGF/RAD51 axis. *eLife* **11**, e75231 (2022).
90. Sun, Y. *et al.* YTHDF1 promotes breast cancer cell growth, DNA damage repair and chemoresistance. *Cell Death Dis* **13**, 230 (2022).

91. Vu, L. P. *et al.* The N6-methyladenosine (m6A)-forming enzyme METTL3 controls myeloid differentiation of normal hematopoietic and leukemia cells. *Nat Med* **23**, 1369–1376 (2017).
92. Barbieri, I. *et al.* Promoter-bound METTL3 maintains myeloid leukaemia by m6A-dependent translation control. *Nature* **552**, 126–131 (2017).
93. Choe, J. *et al.* mRNA circularization by METTL3–eIF3h enhances translation and promotes oncogenesis. *Nature* **561**, 556–560 (2018).
94. Wei, X. *et al.* METTL3 preferentially enhances non-m6A translation of epigenetic factors and promotes tumourigenesis. *Nat Cell Biol* **24**, 1278–1290 (2022).
95. Sorci, M. *et al.* METTL3 regulates WTAP protein homeostasis. *Cell Death Dis* **9**, 796 (2018).
96. Ianniello, Z. *et al.* New insight into the catalytic -dependent and -independent roles of METTL3 in sustaining aberrant translation in chronic myeloid leukemia. *Cell Death Dis* **12**, 870 (2021).
97. Moroz-Omori, E. V. *et al.* METTL3 Inhibitors for Epitranscriptomic Modulation of Cellular Processes. *ChemMedChem* **16**, 3035–3043 (2021).
98. Dolbois, A. *et al.* 1,4,9-Triazaspiro[5.5]undecan-2-one Derivatives as Potent and Selective METTL3 Inhibitors. *J. Med. Chem.* **64**, 12738–12760 (2021).
99. Fiorentino, F., Menna, M., Rotili, D., Valente, S. & Mai, A. METTL3 from Target Validation to the First Small-Molecule Inhibitors: A Medicinal Chemistry Journey. *J. Med. Chem.* **66**, 1654–1677 (2023).
100. Yankova, E. *et al.* Small-molecule inhibition of METTL3 as a strategy against myeloid leukaemia. *Nature* **593**, 597–601 (2021).
101. Sturgess, K. *et al.* Pharmacological inhibition of METTL3 impacts specific haematopoietic lineages. *Leukemia* (2023) doi:10.1038/s41375-023-01965-2.
102. clinicaltrials.gov identifier NCT05584111.

103. Li, Y. *et al*. METTL3 acetylation impedes cancer metastasis via fine-tuning its nuclear and cytosolic functions. *Nat. Commun.* (2022).
104. Mokhtari, RB. *et al.* Combination therapy in combating cancer. *Oncotarget* (2017).
105. Cornet, C. *et al.* ZeOncoTest: Refining and Automating the Zebrafish Xenograft Model for Drug Discovery in Cancer. *Pharmaceuticals* (2019).
106. Siegel, R. *et al.* Cancer Statistics. *American Cancer Society Journals* (2020).
107. Denkert, C. *et al*. Tumour-infiltrating lymphocytes and prognosis in different subtypes of breast cancer: a pooled analysis of 3771 patients treated with neoadjuvant therapy. *Lancet Oncology* (2018).
108. Shi, Y. *et al.* Reduced Expression of METTL3 Promotes Metastasis of Triple-Negative Breast Cancer by m6A Methylation-Mediated COL3A1 Up-Regulation. *Front. Oncol.* (2020).
109. Ruan, H. *et al.* METTL3 Is Suppressed by Circular RNA circMETTL3/miR-34c-3p Signaling and Limits the Tumor Growth and Metastasis in Triple Negative Breast Cancer. *Front. Oncol.* (2021).
110. Chen, C. *et al*. Practical and Scalable Manufacturing Process for the Key Intermediate of Poly(ADP-Ribose) Polymerase Inhibitor Olaparib. *ACS Omega* (2022).
111. Martone, J. *et al*. SMaRT lncRNA controls translation of a G-quadruplex-containing mRNA antagonizing the DHX36 helicase. *EMBO Rep*. 2020
112. Cesari, E. *et al*. Dual inhibition of CDK12 and CDK13 uncovers actionable vulnerabilities in patient-derived ovarian cancer organoids. *J Exp Clin Cancer Res*. 2023

8. LIST OF PUBLICATIONS

- Cesaro B, Iaiza A, Piscopo F, et al. Enhancing sensitivity of triple negative breast cancer to DNA damaging therapy through chemical inhibition of the m6A methyltransferase METTL3. *Cancer Communications* 2023 https://doi.org/10.1002/cac2.12509 (Impact Factor 16.2)

- Coni S, Bordone R, Ivy DM, Yurtsever ZN, Di Magno L, D'Amico R, Cesaro B, Fatica A, et al. Combined inhibition of polyamine metabolism and eIF5A hypusination suppresses colorectal cancer growth through a converging effect on MYC translation. *Cancer Letters*. https://doi.org/10.1016/j.canlet.2023.216120 (Impact Factor 9.7)

- Cesaro B, Tarullo M, Fatica A. Regulation of Gene Expression by m6Am RNA Modification. *Int. J. Mol. Sci.* 2023, 24, 2277. https://doi.org/10.3390/ijms24032277 (Impact Factor 5.6)

- Fernandez Rodriguez G, Cesaro B, Fatica A. Multiple Roles of m6A RNA Modification in Translational Regulation in Cancer. *Int J Mol Sci.* 2022 Aug 11;23(16):8971. doi: 10.3390/ijms23168971 (Impact Factor 5.6)

Seminari:

- 14 ottobre 2022, Probabilistic and epigenetic underpinnings of disease, dr. Pospisilik, seminario EMBL-Sapienza
- 29 novembre 2022, Epigenetic and Epitranscriptomics regulation of neoplastic thymic epithelial cells, dr. Federica Ganci e dr. Alessia Iaiza, seminario IRE-Sapienza
- 5 dicembre, 2022, Exploiting PARP inhibitors combination in the treatment of cancer, prof. Giannini, prof.ssa Bagnato, seminario IFO-Sapienza
- 12 gennaio 2023, "La trascrittomica 3D identifica le interazioni spaziali di singole cellule nei tessuti sani e patologici", prof. Macino, Accademia Medica di Roma
- 9 marzo 2023, Dividere il genoma: meccanismi e disfunzioni, prof. Musacchio, Accademia Medica di Roma
- 6 aprile, 2023, Elucidating and abrogating immunosuppressive mechanisms embodied in the tumor microenvironment, dr. Hanahan, seminario IRE-Sapienza
- 21 aprile, 2023, Spatiotemporal regulation of gene expression: from description to perturbation and back, dr. Legnini, MIT
- 11 maggio 2023, Recognition of cell pathology as a clinically-applicable approach to cancer immunotherapy, dr. Hayday, Accademia Medica di Roma
- 5 giugno 2023, A twist in the protein folding dogma, prof. Bronstein, GBM
- 17 luglio 2023, Structure-based medicinal chemistry optimization of a potent and selective METTL3 inhibitor, dr. Caflisch, Istituto Pasteur
- 13 ottobre 2023, Genetic conflicts during meiosis drive the rapid evolution of chromatin proteins, dr. Malick, seminario EMBL-Sapienza

Corsi di formazione:

- "Corso di formazione teorico-pratico di statistica" marzo 2023, Scuola BeMM
- "Imaging 3D cellular models for biomedical applications" Theoretical-practical course, 10 ottobre 2023, GBM

Congressi:

- SIBBM Seminar "RNA structure, modification, localization and RNA-protein interaction", 20-22 Giugno 2022, Roma (IT)
- 34th Pezcoller Symposium "New Technologies for Studying and Treating Cancer", 19-20 Giugno 2023, Trento (IT)

Pubblicazioni:

- Cesaro B, Iaiza A, Piscopo F, et al. Enhancing sensitivity of triple negative breast cancer to DNA damaging therapy through chemical inhibition of the m6A methyltransferase METTL3. *Cancer Communications* 2023 https://doi.org/10.1002/cac2.12509 (Impact Factor 16.2)

- Coni S, Bordone R, Ivy DM, Yurtsever ZN, Di Magno L, D'Amico R, Cesaro B, Fatica A, et al. Combined inhibition of polyamine metabolism and eIF5A hypusination suppresses colorectal cancer growth through a converging effect on MYC translation. *Cancer Letters*. https://doi.org/10.1016/j.canlet.2023.216120 (Impact Factor 9.7)

- Cesaro B, Tarullo M, Fatica A. Regulation of Gene Expression by m6Am RNA Modification. *Int. J. Mol. Sci.*

2023, 24, 2277. https://doi.org/10.3390/ijms24032277 (Impact Factor 5.6)

- Fernandez Rodriguez G, Cesaro B, Fatica A. Multiple Roles of m6A RNA Modification in Translational Regulation in Cancer. *Int J Mol Sci*. 2022 Aug 11;23(16):8971. doi: 10.3390/ijms23168971 (Impact Factor 5.6)

Mobilità internazionale

During my third year of PhD, I had the opportunity to spend a month in Professor Rios' laboratory at the Prinses Maxima Centrum in Utrecht (Netherlands), thanks to the funding from my doctoral program and the "Scientific Exchange Grant" provided by the EMBO organization, of which I was awarded as winner. The research group had access to 45 lines of breast cancer organoids derived from patients with triple-negative breast cancer (TNBC). I developed the ability to culture and plate various organoid lines, adjusting the splitting ratio that best suited each line. Moreover, I conducted immunostaining on a set of lines to assess the differential expression of basal and luminal markers (K14, K8), employing confocal microscopy to study three-dimensional structures such as organoids. Finally, I actively participated in Journal Clubs and laboratory meetings organized by the group, integrating with the projects of other laboratory members.

9. POINT BY POINT RESPONSE TO REVIEWERS

1st Reviewer: Alessandro Michienzi
Accept as is

Dr. Bianca Cesaro's thesis investigates the effectiveness of inhibiting the catalytic activity of the METTL3 enzyme, which mediates m6A RNA methylation, using specific small molecules (STM2457) as a treatment for a highly aggressive type of breast cancer known as Triple-negative breast cancer (TBNC). The experimental questions were well-defined by the candidate, and the methods chosen to test the hypotheses are suitable for this type of study. The thesis is original with a clear writing style. The experiments are well-described and well-supported by statistical analyses. The references are appropriate. The work is discussed appropriately. The reported work makes a valuable contribution to an area of research focused on identifying new targets and specific therapeutic molecules for breast cancer treatment. In summary, the thesis presents excellent experimental work, the extent and quality of which justifies its submission to the evaluating committee.

I thank the reviewer for evaluating my PhD thesis. I appreciate the time and effort they took to provide me with valuable feedback.

2nd Reviewer: Silvia Di Agostino
Minor Revision

This thesis titled “Enhancing sensitivity of triple-negative breast cancer to DNA damaging therapy through chemical inhibition of the m6A methyltransferase METTL3” was proposed by PhD student Bianca Cesaro. This is a very good doctoral thesis in which the rationale is supported by in vitro and in vivo experiments and

massive sequencing in different in vitro conditions. It is therefore a study supported by an effort of many scientific skills where in the dissertation phase, the candidate should emphasize her own work. In general, the whole thesis is well written. From the point of view of the content, in the literature (pubmed) there are to date only 6 papers published including the keywords METTL3 and TNBC, therefore the candidate has identified a very hot topic with future therapeutic prospects in this neglected subgroup of BC. However, the papers cited above (doi: 10.3389/fonc.2020.01126; doi: 10.3389/fonc.2021.778132. figure 1 and 2; https://doi.org/10.1016/j.gene.2019.144076 just to cite a few examples) reported a downregulation of METTL3 transcript in TNBC. Since the foundational experiments on a large panel of BC cells and obviously the functional and molecular experiments are extremely convincing and showed high technical quality, the candidate should discuss this discrepancy with the published paper in the discussion, also in light of a future refereeing of the possible manuscript.

I thank the reviewer for carefully reading my PhD thesis and for the suggestion. I have discussed the discordant papers mentioned by the reviewer and included the references cited above in the bibliography section of my thesis. In brief, despite the majority of evidences in literature show METTL3 as a oncogene in most cancer types, including triple-negative breast cancer, it was also reported as tumor suppressor in some cases, suggesting how context-dependent and environmental factors may significantly infer study outcomes. This highlights the intricate and contradictory roles of METTL3, as well as other m^{6}A members, emphasizing the need for a more comprehensive understanding of the m^{6}A regulatory landscape.

Minor observations:
- In the text when “TIL” appears for the first time, please, insert the meaning of the acronym in brackets (Tumor Infiltrating Lymphocytes)

I thank the reviewer for the observation. However, “TIL” appears for the first time, along with its extended meaning “Tumor Infiltrating Lymphocytes”, on pag.16 of my thesis.